Version of Record: https://www.sciencedirect.com/science/article/pii/S1387380616302494
Manuscript_783ec196fb5046dd4baf1284525688bb

Calculation of the sensitivity of proton-transfer-reaction mass spectrometry (PTR-MS) for organic trace gases

Kanako Sekimoto[1,2]*, Shao-Meng Li[3], Bin Yuan[1,4], Abigail Koss[1,4,5], Matthew Coggon[1,4], Carsten Warneke[1,4], Joost de Gouw[1,4,5]

[1] Chemical Sciences Division, NOAA Earth System Research Laboratory, Boulder, CO, USA

[2] Graduate School of Nanobioscience, Yokohama City University, Yokohama, Japan

[3] Air Quality Process Research Division, Science and Technology Branch, Environment and Climate Change Canada, Toronto, Canada

[4] Cooperative Institute for Research in Environmental Sciences, University of Colorado Boulder, Boulder, CO, USA

[5] Department of Chemistry and Biochemistry, University of Colorado, Boulder, CO, USA

*Corresponding author

Chemical Sciences Division, NOAA Earth System Research Laboratory

325 Broadway, R/CSD7, Boulder, CO 80305 USA

Tel: +1-303-497-6055

E-mail: kanako.sekimoto@noaa.gov

Graphical abstract for "Calculation of the sensitivity of proton-transfer-reaction mass spectrometry (PTR-MS) for organic trace gases using molecular properties"

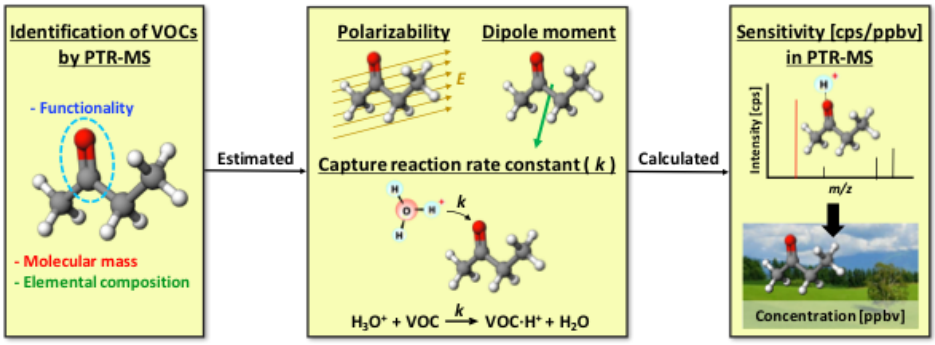

Research highlights for "Calculation of the sensitivity of proton-transfer-reaction mass spectrometry (PTR-MS) for organic trace gases using molecular properties"

- Correlation between rate constant and sensitivity in PTR-MS was investigated. (79)
- Measured sensitivities were linearly correlated with kinetic rate constants. (78)
- Kinetic rate constants were accurately estimated from molecular properties. (77)
- Sensitivities calculated from estimated rate constants had an accuracy with 20-50%. (85)

Abstract

Proton-transfer-reaction mass spectrometry (PTR-MS) allows the detection of a large number of trace gases in air through proton-transfer reaction with H_3O^+ reagent ions and detection by a mass spectrometer. Measurement sensitivities can be experimentally determined using calibration gases or calculated using the rate constant for the proton-transfer reaction, but rate constants have only been measured for a subset of compounds. The average-dipole-orientation (ADO) theory describes how collision rate constants between an ion and neutral molecules are accurately obtained using the polarizability and dipole moment of the molecule. Here we show that polarizability, dipole moment, and resulting ADO rate constants for proton-transfer reactions of H_3O^+ with various different volatile organic compounds (VOCs) can be obtained using the molecular mass, elemental composition, and functionality of VOCs. The polarizabilities of a class of VOCs possessing specific number of electronegative atoms were linearly correlated with their molecular mass. The dipole moments in a series of VOCs, in which VOCs contain a specific functional group and arbitrary residual hydrocarbon parts, were approximated as a constant value. The ADO rate constants calculated using polarizability and dipole moment, as estimated from molecular mass, elemental composition, and functional group, agreed within 10 % with measured values for most VOCs. Those ADO rate constants were applied to the calculation of the sensitivities of VOCs detected by our PTR-MS, taking into account the ion transmission efficiency and the degree of fragmentation of protonated VOCs observed in that instrument. The resulting calculated sensitivities agreed within 15 % with the measured ones. This result shows that the neutral concentration of a VOC detected as protonated molecule in PTR-MS can be determined using only molecular mass, elemental composition, and functionality of the VOC. The present study is useful for all PTR-MS instruments regardless of the type of mass analyzer; however, the identification of elemental composition by high mass resolution instrumentation is important.

Keyword: Proton-transfer-reaction mass spectrometry (PTR-MS), Volatile organic compound (VOC), Average-dipole-orientation (ADO) theory, Reaction rate constant, Hydronium ion H_3O^+

Introduction

Volatile organic compounds (VOCs) in the atmosphere are emitted from different biogenic and anthropogenic sources. The production, storage, and use of fossil fuel products, as well as intensive agriculture and biomass burning, all perturb the natural atmospheric composition. Deposition processes and various chemical reactions remove and change the VOC composition in the atmosphere on time scales from minutes to months. Traditional analytical methodologies (e.g., gas chromatographic methods) have been developed for VOC measurements: however, they require sample preparation and accumulation over some periods of time. Proton-transfer-reaction mass spectrometry (PTR-MS) allows real-time, on-line measurements of atmospheric VOCs with a high sensitivity and fast response time, and has overcome some of the disadvantages of traditional methodologies with low time resolution [1-3]. Furthermore, recently available PTR-MS instruments that use time-of-flight (ToF) mass analyzers with high mass resolution facilitate the separation of nominally isobaric species [4,5], which increases the number of measureable atmospheric VOCs (> 100 species) and reduces possible chemical interferences [6]. PTR-ToF-MS has quickly become a well-established analytical technique for *in-situ* VOC measurements utilized in a wide variety of fields such as atmospheric chemistry [6,7], medical and biotechnological applications [8], and food and flavor sciences [9,10].

The PTR-MS technique is based on chemical ionization through proton-transfer reactions of VOCs with hydronium ions H_3O^+, which takes place in the sample gas flowing through a low-pressure drift tube [2]. VOCs in the sample gas with higher proton affinities than H_2O (691.0 kJ mol^{-1} [11]) can be ionized via proton transfer with H_3O^+, as follows:

$$H_3O^+ + VOC \rightarrow VOC{\cdot}H^+ + H_2O \qquad (1)$$

This reaction includes many atmospherically important VOCs, such as (un)saturated and aromatic hydrocarbons (except for alkanes smaller than C5) and VOCs containing oxygen, nitrogen and sulfur [11]. The resulting protonated VOCs ($VOC{\cdot}H^+$) are detected by a mass analyzer. The concentration of a neutral VOC is typically determined by calibrating an instrument with a standard of known concentration and recording the response of the protonated VOC ($VOC{\cdot}H^+$). The most accurate results are obtained when the PTR-MS instrument is calibrated for each single VOC. However, this process is labor-intensive and it is not always feasible to develop accurate standards for every VOC detected by PTR-MS. This is especially true for high-resolution PTR-ToF-MS instruments since these instruments allow for the detection of a much larger number of VOC species. The atmosphere contains hundreds of thousands of compounds; some of these have yet to be identified [12]. This emphasizes that not every compound can be calibrated for, especially since no commercial standards are available for a large number of compounds.

The sensitivity of a given VOC of a PTR-MS can also be calculated using the measured ion counts of $VOC{\cdot}H^+$ and H_3O^+, the rate constant for the proton-transfer reaction (1), and the drift tube conditions (its length, pressure, temperature, etc.) [2]. Reaction (1) is exothermic and fast for those

compounds that have proton affinities higher than that of H_2O; under such conditions, the reaction proceeds at a rate close to the collision rate of a few times 10^{-9} cm^3 $molecule^{-1}$ s^{-1}. It has been known that such collision rate constants can be accurately calculated by the average-dipole-orientation (ADO) theory involving analytical and numerical methods [13,14]. Several groups have reported lists of proton-transfer reaction rate constants between H_3O^+ and atmospheric VOCs using the ADO theory [15,16]. Such theoretical approaches have frequently required quantum chemical calculations to determine the fundamental factors in the ADO theory, i.e., polarizabilities and dipole moments of individual VOCs, because of the limited experimental results. Such computational work is time-consuming in itself, but can partially overcome the practical difficulty of developing calibration procedures for certain VOCs of interest or for more exotic VOCs such as reaction intermediates that cannot be obtained commercially in pure form.

In the present paper, we first discuss how the sensitivities in PTR-MS are correlated with reaction rate constants, by using the experimentally determined sensitivities of selected VOCs as the basis for the discussion. Secondly, we show that the polarizability and permanent dipole moment of various VOCs can be accurately estimated using their molecular mass, elemental composition, and functionality. Molecular mass and elemental composition of a VOC are directly determined by PTR-MS (in some cases, high mass resolution analyzers are required) and functionality can often be inferred from the degree of unsaturation and external conditions such as the type of analyte, other ions in the mass spectra, concurrent gas chromatography measurements, etc. Using the resulting polarizability and dipole moment in the ADO theory, we show that one can accurately calculate proton-transfer reaction rate constants for atmospherically important VOCs, without the aforementioned extensive computational investigations. Finally, we will show how well sensitivities of the VOCs in a PTR-MS can be calculated using measured or ADO rate constants, by comparing with those that were experimentally determined, according to the scenarios described below and Scheme 1:

1. Calculate sensitivity from measured rate constant and its accuracy, or
2. Calculate sensitivity from ADO rate constant determined by measured polarizability and dipole moment and its accuracy, or
3. Calculate sensitivity from ADO rate constant determined by polarizability and dipole moment estimated using molecular mass, elemental composition, and functionality and its accuracy

(Scheme 1)

2. Data collection

2.1. Sensitivity of VOCs in PTR-MS

The sensitivities of various VOCs were determined by the following 3 different instruments: (1) a chemical ionization time-of-flight mass spectrometer (H_3O^+-ToF-CIMS, Aerodyne Research Inc. MA, USA; Tofwerk AG, Thun, Switzerland), (2) a modified version of this same instrument (modified H_3O^+-ToF-CIMS), and (3) a PTR-MS with a quadrupole mass analyzer (PTR-QMS). The instruments have been described in detail elsewhere [7,17,18]. Those 3 instruments all consist of (i) a hollow cathode reagent ion source to form H_3O^+ reagent ions, (ii) a drift tube reaction region where proton-transfer reactions between H_3O^+ and neutral molecules take place, and (iii) a mass analyzer. The H_3O^+-ToF-CIMS instrument has two RF-only segmented quadrupole ion guides between the drift tube and mass analyzer, whereas the modified instrument has one ion guide. The drift tube conditions for the 3 instruments (length, pressure, temperature, voltage, and resulting E/N ratio) are summarized in Table 1a. In this study, measured sensitivities of the 11 VOCs listed in Table 2 will be used. The calibration of those VOCs for the 3 instruments were performed utilizing standard mixtures in gas cylinders, in which measurement accuracies are within 20 %.

(Table 1) and (Table 2)

2.2. Product ion distribution of protonated VOCs

In order to obtain the product ion distributions of protonated molecules for the VOCs listed in Table 2, a gas chromatograph (GC) instrument was used as an interface to the (modified) H_3O^+-ToF-CIMS and PTR-QMS. The GC collected the VOCs in a liquid nitrogen cryotrap or PFA (perfluoro alkoxy) Teflon tube maintained at low temperature, and then VOCs were separated by capillary columns. The column eluent was directed to the inlet of the ToF-CIMS or PTR-QMS. The setups of GC-ToF-CIMS and GC-QMS have been described in detail by Koss et al. [19] and Warneke et al. [17], respectively.

2.3. Polarizability, permanent dipole moment, and reaction rate constant

The values of polarizability volume for 288 compounds without/with several electronegative atoms, such as oxygen O, nitrogen N and sulfur S, were taken from the CRC Handbook [20]. Polarizabilities are mostly determined by measurements of a dielectric constants or refractive indices of compounds, and from quantum chemical calculation using the density function theory-B3LYP [15]. For permanent dipole moments, the values for 349 polar compounds experimentally determined by microwave spectroscopy, molecular beam electric resonance, and high-resolution spectroscopic, as well as from measurements of the dielectric constant were also taken from the CRC Handbook [20]. Thermal rate constants for sufficiently

exothermic proton-transfer reactions between H_3O^+ and 110 compounds, whose proton affinities are more than 20 kJ mol^{-1} higher than H_2O, at 300 K were taken from literature on flowing afterglow and/or selected ion flow tube mass spectrometry studies [16,21-33], part of which also used the parameterized trajectory calculations [14], and PTR-MS studies [1,34]. The VOCs included in this study are classified by functional group, residual hydrocarbon part, and elemental composition. We use the acronym HCP_m to denote different compound classes according to elemental composition, where *P* and *m* represent the species and number of electronegative atoms included in the compounds, respectively, and HC stands for the hydrocarbon part. The detailed information for the compounds whose dipole moments, polarizabilities, and rate constants are included are summarized in Tables 3 – 5, respectively.

(Table 3), (Table 4), and (Table 5)

3. Results and discussion

3.1. Correlation between reaction rate constant and measured sensitivity in PTR-MS: the instrument function

It has been shown that the sensitivity of a VOC in PTR-MS is correlated with the reaction rate constant for proton transfer with H_3O^+ [2]. When it is assumed that proton-transfer reaction (1) between the abundant H_3O^+ reagent ions and a trace VOC convert a small fraction of H_3O^+ into protonated molecule $VOC{\cdot}H^+$, the concentration of $VOC{\cdot}H^+$ ions formed ($[VOC{\cdot}H^+]$) can be calculated as follows:

$$[VOC{\cdot}H^+] \approx k\,[H_3O^+]\,[VOC]\,\Delta t \qquad (2)$$

where k is the rate constant [cm^3 $molecule^{-1}$ s^{-1}], $[H_3O^+]$ and [VOC] are the concentrations of the H_3O^+ ions and trace VOC in the drift tube, respectively, and Δt is the reaction time [s] for H_3O^+ traversing the drift tube. This equation shows that the density of $VOC{\cdot}H^+$ ions at the end of the drift tube is linearly related to the concentration of the VOC. The protonated molecules $VOC{\cdot}H^+$ can be fragmented during proton transfer, for example protonated isoprene and α-pinene (see Table 2c). The reduced concentration of $VOC{\cdot}H^+$ due to fragmentation is expressed by using the residual fraction of $VOC{\cdot}H^+$ in the drift tube ($F_{VOC{\cdot}H^+}$), i.e.,

$$[VOC{\cdot}H^+] = k\,[H_3O^+]\,[VOC]\,\Delta t\,F_{VOC{\cdot}H^+} \qquad (3)$$

The reaction time Δt is determined by the drift tube conditions:

$$\Delta t = \frac{L}{v_d} = \frac{L}{\mu E} = \frac{L}{\mu_0 N_0} \times \frac{N}{E} \qquad (4)$$

In this equation, L is the length [cm] of the drift tube, v_d the drift velocity [cm s^{-1}], μ (μ_0) the (reduced) mobility [cm^2 V^{-1} s^{-1}] of H_3O^+, N_0 the gas number density at standard pressure (1 atm) and temperature (273.15 K) 2.6868 x 10^{19} [molecule cm^{-3}], N the number density [molecule cm^{-3}] of the gas in the drift tube, and E the electric field [V cm^{-1}] in the drift tube. Using Eqs. (3) and (4), the fraction of H_3O^+ that is converted into $VOC{\cdot}H^+$ ions can be expressed as:

$$\frac{[VOC{\cdot}H^+]}{[H_3O^+]} = k \times [VOC] \times \frac{L}{\mu_0 N_0} \times \frac{N}{E} \times F_{VOC{\cdot}H^+} \quad (5)$$

To simplify, the other factors that affect the ratio $[VOC{\cdot}H^+]/[H_3O^+]$ at the end of the drift tube, such as diffusion coefficients depending on individual ion species [35,36], are not included here. A fraction of H_3O^+ and $VOC{\cdot}H^+$ ions are sampled into the mass analyzer through ion guides and detected by a detector. The resulting ion intensities (in counts-per-second; cps), $I_{H_3O^+}$ for H_3O^+ and $I_{VOC{\cdot}H^+}$ for $VOC{\cdot}H^+$ ions, are related to the quantity to the volume-mixing ratio (= [VOC]/*N*) by

$$\frac{I_{VOC{\cdot}H^+}}{I_{H_3O^+}} = \frac{[VOC{\cdot}H^+]}{[H_3O^+]} \times \frac{T_{VOC{\cdot}H^+}}{T_{H_3O^+}} = \frac{[VOC]}{N} \times k \times \frac{L}{\mu_0 N_0} \times \frac{N^2}{E} \times F_{VOC{\cdot}H^+} \times \frac{T_{VOC{\cdot}H^+}}{T_{H_3O^+}} \quad (6)$$

The factors $T_{VOC{\cdot}H^+}$ and $T_{H_3O^+}$ are the transmission efficiencies for $VOC{\cdot}H^+$ and H_3O^+, respectively. These are determined by (i) the extraction efficiency of ions from the drift tube into the mass analyzer, (ii) the transmission efficiency of the analyzer, and (iii) the detection efficiency of the detector for each mass. From Eq. (6), the measured sensitivity in PTR-MS is defined as the ion intensity of $VOC{\cdot}H^+$ obtained at a volume-mixing ratio of 1 ppbv (parts per billion by volume; 10^{-9}) and normalized to a H_3O^+ ion intensity ($I_{H_3O^+}$) of 10^6 cps [2]:

$$Sens_{meas.}\,[ncps\ ppbv^{-1}] = \frac{\frac{I_{VOC{\cdot}H^+}}{I_{H_3O^+}} \times 10^6\,[ncps]}{\frac{[VOC]}{N}\,[ppbv]} = k \times A \times F_{VOC{\cdot}H^+} \times \frac{T_{VOC{\cdot}H^+}}{T_{H_3O^+}} \quad (7\text{-a})$$

$$A = 10^{-3} \times \frac{L}{\mu_0 N_0} \times \frac{N^2}{E} \quad (7\text{-b})$$

where "ncps" corresponds to normalized counts-per-second. The normalization to the H_3O^+ ion intensity removes variability due to fluctuations in the ion source and detector. The fraction of $VOC{\cdot}H^+$ ($F_{VOC{\cdot}H^+}$) and the transmission efficiencies ($\frac{T_{VOC{\cdot}H^+}}{T_{H_3O^+}}$) in Eq. (7-a) depend on the species or molecular mass of a VOC, while the factor *A* is a VOC independent constant value that is determined by the drift tube conditions as described in Eq. (7-b). Equation (7-a) suggests that if the measured sensitivity ($Sens_{meas.}$) originating from the detected ion intensities of $VOC{\cdot}H^+$ and H_3O^+ ($I_{VOC{\cdot}H^+}$ and $I_{H_3O^+}$) is corrected for fragmentation and transmission efficiencies, the resulting sensitivity should be linearly dependent on the reaction rate

constant *k*. This means that the sensitivity can be calculated from the rate constants, if the instrument factors (H_3O^+ ion intensity, fragmentation, and transmission efficiency) are determined accurately.

In the following we investigate the linear relationship of the sensitivities with the rate constants for the 11 VOCs in the 3 different instruments (Fig. 1). The vertical axis in Fig. 1 shows the corrected sensitivities ($Sens_{corr.}$ in Table 2b-II), which are obtained using the measured sensitivities ($Sens_{meas.}$), the fraction of $VOC{\cdot}H^+$ ($F_{VOC{\cdot}H^+}$), and the ion transmission efficiency ($\frac{T_{VOC{\cdot}H^+}}{T_{H_3O^+}}$), as follows:

$$Sens_{corr.}\,[ncps\ ppbv^{-1}] = Sens_{meas.}\,[ncps\ ppbv^{-1}] \times \frac{100}{F_{VOC{\cdot}H^+}\,[\%]} \times \frac{T_{H_3O^+}}{T_{VOC{\cdot}H^+}} \quad (8)$$

$Sens_{meas.}$, $F_{VOC{\cdot}H^+}$, and $\frac{T_{VOC{\cdot}H^+}}{T_{H_3O^+}}$ for each instrument are summarized in Tables 2b-I, 2c, and 1a, respectively. The reaction rate constants for the VOCs used here are measured at 300 K, as shown in Table 2d. Figure 1 suggests that the sensitivities of all the VOCs except for methanol are described well by a linear function (Eq. 9) of reaction rate constant $k_{T=300K}$, regardless of the type of instrumentation.

$$Sens_{corr.}\,[\text{ncps ppbv}^{-1}] = a \times k_{T=300K} + b \quad (9)$$

The deviation of methanol from linear correlation is discussed later.

(Figure 1)

According to Eqs. (7-a) and (9), the slope *a* corresponds to the factor *A* in Eq. (7-a), whereas the intercept *b* should be zero, respectively. The factor *A* was calculated using the drift tube conditions shown in Table 1a and the literature value of the reduced mobility $\mu_0 = 2.76$ [$cm^2\ V^{-1}\ s^{-1}$] [39]. The resulting *A* values for the individual instruments are summarized in Table 1b. The agreement in values between the slope *a* and factor *A* for the PTR-QMS is good (an error less than 20 %), while that for the (modified) H_3O^+-ToF-CIMS instruments do not agree as well (errors over 50 %). The significant disagreement for the ToF-CIMS can come from specific uncertainties of the factor *A*, which are caused by the quadrupole ion guides. Previous work using the H_3O^+-ToF-CIMS instrument [7] reported the occurrence of chemical reactions inside the ion guides. This suggests that the reaction time Δt as described by Eq. (4) needs to be increased to account for the added reaction time in the ion guides, resulting in an increase in the

value of the factor *A* (Eq. 7-b). However, ion guide conditions were not included in the calculations of Δ*t* and *A* presented here. Additionally, the transmission efficiency $\frac{T_{H_3O^+}}{T_{VOC\cdot H^+}}$ used in Eq. (8) is expected to have significant uncertainties because its determination as a function of *m/z* value of $VOC\cdot H^+$ is not straightforward [7].

The deviation of the intercept *b* from zero is observed regardless of the type of instrument. A potential source for this deviation is the use of the thermal rate constants to obtain the linear function (Eq. 9). The rate constants were determined at 300 K, which is different from the collision conditions in the drift tube. According to the Wannier equation [39], the total kinetic energies of the H_3O^+ reagent ions accelerated in the drift tubes used here are 0.5 – 1.0 eV, which are rather high compared to the thermal energy. Therefore, the actual proton-transfer reactions between the H_3O^+ reagent ion and VOCs in the drift tube should proceed kinetically. Viggiano et al. [40] reported the kinetic energy dependence on reaction rate constant by using a selected ion flow drift tube. They found that the degree of the change in rate constant with varying the kinetic energy is dependent on the species of neutral molecule involved in the reaction with a definite ion. Therefore, the question is how large the proton-transfer reaction rate constants between H_3O^+ and individual VOCs depend on the kinetic energy. However, it should be noted that the thermal reaction rate constants are applicable to estimate the linear relationship between the sensitivity and rate constant in PTR-MS by taking into account the intercept, as shown in Fig. 1. In other words, the use of the thermal rate constant and intercept *b* in Eq. (9) leads to an accurate determination of linear correlation of sensitivity with rate constant for a given PTR-MS instrument. It suggests that if the thermal rate constants of VOCs detected in the PTR-MS are given, their sensitivities can be calculated only by substituting those rate constants in the instrument function (Eq. 9) determined using selected standard VOCs.

Figure 1 shows that methanol gives a lower sensitivity relative to the corresponding rate constant in all the instruments. This is due to significantly large uncertainties of the transmission efficiency inside quadrupole sectors for protonated methanol and its product ions. As protonated methanol CH_5O^+ and its major product ion CH_3^+ have low mass (*m/z* 33 and 15, respectively), those ions have large mass discrimination effect inside the quadrupole sectors in the individual instruments. This amplifies the uncertainty of the factors $F_{VOC\cdot H^+}$ and $\frac{T_{H_3O^+}}{T_{VOC\cdot H^+}}$ used in Eq. (8), and possibly explains the lower than expected sensitivity. Consequently, VOCs with large uncertainties of fragmentation and ion transmission efficiencies should be avoided to determine the instrument function (Eq. 9).

In the next section, we discuss a method to estimate the thermal proton-transfer reaction rate constants between H_3O^+ and VOCs using molecular properties.

3.2. Calculation of the reaction rate constants between H_3O^+ and specific VOCs

In order to accurately calculate collision rate constants between an ion and neutral molecule, various theoretical approaches have been developed. The first theory was proposed by Langevin in 1905 [41], which provides a good approximation of the rate constants for nonpolar molecules. The Langevin rate constants ($k_{Langevin}$) are calculated based on the polarizability α of a given neutral molecule R:

$$k_{Langevin} = 2\pi q\ \alpha^{1/2}\ (M_R^{-1} + M_{ion}^{-1})^{1/2} \quad (10)$$

where q is the charge of the ion, M_R the mass of molecule R, and M_{ion} the mass of the ion. A better approximation, which accounts for the effects of a permanent dipole moment of the polar molecule and the orientation of the dipole in the molecule with respect to the ion, is the average-dipole-orientation (ADO) theory, first developed by Su and Bowers in 1973 [13]. This theory is the basis of the numerical trajectory parameterization which makes it possible to correctly describe the kinetic energy dependence of the cross sections for exothermic reactions at center-of-mass energies below 0.3 eV [14,42].

In the most classical ADO theory [13], the rate constants (k_{ADO}) of the proton transfer reaction of H_3O^+ with a given molecule R can be analytically calculated from (i) the polarizability α, (ii) the permanent dipole moment μ_D, and (iii) the locking constant C, as follows:

$$k_{ADO} = 2\pi q\,(M_R^{-1} + M_{ion}^{-1})^{1/2}\,[\alpha^{1/2} + C\,\mu_D\,(2/\pi k_B T)^{1/2}]$$
$$= k_{Langevin} \times \left[1 + \frac{C\,\mu_D\,(2/\pi k_B T)^{1/2}}{\alpha^{1/2}}\right] \quad (11)$$

where k_B and T are the Boltzmann constant and temperature, respectively. In this section, we investigate how accurately the fundamental factors in Eq. (11), i.e., polarizability α and dipole moment μ_D, can be estimated using only the molecular mass, elemental composition, and functionality of molecules R. Furthermore, the locking constant C suitable for the calculation of the exothermic proton-transfer reaction rate constants between H_3O^+ and various VOCs is estimated.

3.2.1. Polarizability

It is known that the polarizability of a compound R, which is the response of the electron cloud to an external electric field, is related to the molecular mass by the Debye equation (Eq. 12):

$$\alpha = \frac{3}{4\pi r N_A}\left(\frac{\varepsilon_r - 1}{\varepsilon_r + 2}\right) M_R - \frac{\mu_D^2}{12\pi\varepsilon_0 k_B T} \qquad (12)$$

where α denotes the polarizability volume [m^3], ρ the mass density [kg m^{-3}], N_A the Avogadro constant 6.022 x 10^{23} [mol^{-1}], ε_r the relative permittivity [dimensionless], M_R the molecular mass [kg mol^{-1}], μ_D the permanent dipole moment [C m], ε_0 the vacuum permittivity 8.854 x 10^{-12} [C^2 J^{-1} m^{-1}], k_B the Boltzmann constant 1.380 x 10^{-23} [J K^{-1}], and T the temperature [K] at which the permanent dipole of the molecule rotates. The values of ε_r and μ_D are strongly dependent on the polarity, which is partly governed by the number and type of functional groups present in the neutral. The correlation between polarizability and molecular mass is investigated for the individual compound categories of HCP_m shown in Table 3a. The number and chemical properties of species used in each compound category are summarized in Tables 3b and c, respectively. Figures 2a-h show the literature values of polarizability [15,20] plotted as a function of molecular mass for the classes of compounds in Table 3. All of the figures clearly show that within each class of compounds, the polarizability can be described by a linear function (Eq. 13) of molecular mass with a very high correlation coefficient r ($r \geq 0.9536$).

$$\alpha = c \times M_R + d \quad \text{(coefficients } c \text{ and } d \text{ depend on elemental composition)} \qquad (13)$$

The linear functions obtained using the averages of literature data and corresponding correlation coefficients are summarized in Table 3d. There were several notable exceptions as indicated by filled symbols in Figs. 2a and d-g. The polarizabilities of the compounds having π-conjugated systems and/or symmetric structures tend to be higher than those of other compounds in the respective groups, as seen on azulene, phenanthrene, pyrene, fluoranthene, cyanogen, fumaronitile, and *p*-dicyanobenzene (see Fig. 2i). Conjugated system leads to electron delocalization, resulting in significantly enhanced responses of the electron cloud. The high polarizability for the symmetrically-structural compound might be due to relatively low dipole moment, which results in a negligibly small value of the second term in the Debye equation (Eq. 12). The reasons for the significant deviation in polarizability of naphthacene, paraldehyde, butylamine, and tetranitromethane are unknown.

(Figure 2)

It should be noted here that the slope *c* and intercept *d* in Eq. (13) correspond to the first and second terms in the Debye equation (Eq. 12), respectively. That is, the factors ρ, ε_r and μ_D in Eq. (12) can be assumed as constants for the individual HCP_m categories, indicating that the dependence of the polarizability on the molecular mass is significantly stronger than on the density, permittivity and dipole moment. This result is consistent with the later discussion in Section 3.2.2, where it is shown that the dipole moments of compounds possessing the same chemical class are approximately constants. The polarizability calculated using the molecular mass and the linear function for each HCP_m category shown in Table 3d, denoted as $\alpha(M_R, \text{HC}P_m)$, were compared with those determined by measurements ($\alpha_{meas.}$ [20]). The average relative errors (in %) of $\alpha(M_R, \text{HC}P_m)$ with respect to $\alpha_{meas.}$ for individual compound categories were 2.7 – 10.8 % as seen in Table 3f, while the distributions of those relative errors were within ≈ 15 % (Fig. S-1). These results show that if the polarizability of a compound is unknown, it can be estimated with good accuracy from the mass and the measured composition of a compound, both of which can be determined by mass spectrometry.

If the composition of VOCs cannot be determined by nominal mass measurement, the polarizabilities of such compounds are estimated from their molecular mass only, denoted as $\alpha(M_R)$. The equation for $\alpha(M_R)$, shown in Table 3e, was obtained by averaging the coefficients *c* and *d* for each HCP_m category shown in Table 3d. The errors of $\alpha(M_R)$ relative to $\alpha_{meas.}$ are larger compared to those of $\alpha(M_R, \text{HC}P_m)$. The average errors of $\alpha(M_R)$ are 5.0 – 26.2 % for individual compound categories (Table 3g) and the distributions of those errors have the peak around 10 % but spread up to 70 % (Fig. S-2).

3.2.2. Permanent dipole moment

The permanent dipole moment μ_D of a compound R results from the partial charges on the atoms that arise from differences in electronegativity or other features of bonding (e.g., structural symmetry). When the centers of positive and negative charges in the molecule, which have equal magnitude *q* [C], are separated by a distance *l* [m], the magnitude of μ_D [in Debye; 1 D = 3.3564 x 10^{-30} C m] established is given by the following equation:

$$\mu_D = q \times l \qquad (14)$$

The dipole moment μ_D of nonpolar compounds with elemental composition HC are typically lower than 1 D. In this case, the effect of the dipole moment on the collision rate constant is negligible, and therefore, the dipole moments of HC can be approximated as zero. Here the relationship between the dipole moment of a polar compound R and its physicochemical properties, e.g., molecular mass, chemical properties characterized by functional group and residual hydrocarbon part, was investigated for various VOCs with several electronegative atoms of O, N and S. It is found in the present work that dipole moments in a certain class of compounds are relatively constant. Figures 3a – e show measured dipole moment values ($\mu_{D\ meas.}$ [20]) plotted as a function of molecular mass for compounds in different categories of composition HCP_m and functional group. The number of compounds and their chemical properties are summarized in Table 4c. Bars put on some data points in Figs. 3a – e represent the range in values of $\mu_{D\ meas.}$ for regio-isomers and/or stereo-isomers (e.g., *ortho*-, *meta*- and *para*-isomers, and/or *cis*-, *trans*-, *gauche*- and *anti*-isomers, respectively). The maxima and minima of the individual bars show the maximum and minimum $\mu_{D\ meas.}$ values for the isomers, respectively, while the data points indicate the average values in these cases. It should be noted in Figs. 3a – e that the dipole moment of a class of compounds possessing a specific functional group can be approximated as a constant, independent of their molecular mass (Eq. 15). Furthermore, standard deviations in the dipole moment within a class of compounds are relatively small.

$$\mu_D = K \qquad (15)$$

where K is a constant depending on the functional group.

(Figure 3)

Some compounds, represented as the filled data points in Figs. 3a, b, c, and e, have significantly different dipole moments from the other compounds in that group. Those deviations are likely due to the specific properties of the hydrocarbon parts in the compounds. In the case of formaldehyde (Fig. 3a), hydrogen cyanide (Fig. 3c) and hydrogen isocyanide (Fig. 3c), which have lower dipole moments than other compounds in their respective groups, the hydrocarbon parts excluding the functional groups contain only one hydrogen atom (see Fig. 3f). Such properties lead to shorter distances between the positive and negative charges in those compounds compared with the others having larger hydrocarbon parts, resulting in a lower dipole moment according to Eq. (14). The exceptions at higher dipole moment in the ketone/aldehyde series (Fig. 3a), i.e., *trans*-2-butenal, 3-methyl-2-cyclopenten-1-one and 2,4,6-cycloheptatrien-1-one, are enones, i.e. alkenes conjugated to ketones (Fig. 3f). Conjugated system and resulting electron delocalization can enhance the polarity of a carbonyl group. The other 3 exceptions, i.e., benzyl acetate (Fig. 3b), *N*,*N*-

dimetylaniline (Fig. 3c) and benzenthiol (Fig. 3e), are aromatic compounds (Fig. 3f). The significantly different dipole moments for those compounds may be caused by the interactions between individual functional group and resonance structures of the aromatics. In addition, compounds with symmetric structures are expected to have relatively low dipole moments because of overlapping distributions of positive and negative charges, i.e., $l = 0$ in Eq. (14), leads to $\mu_D = 0$, although such compounds were not included in the data shown in Fig. 3.

According to Eq. (15), the constant value representing dipole moments of a class of compounds with a specific functional group, denoted as μ_D(FG), was obtained by calculating the average values of $\mu_{D\ meas.}$ of the compounds in the individual functional group series (Table 4d), and were compared with $\mu_{D\ meas}$. The average values and distributions of the relative errors (in %) of μ_D(FG) with respect to $\mu_{D\ meas.}$ for the categories of individual functional groups and composition HCP_m are shown in Table 4g and Fig. S-3, respectively. The relative errors for all of the compound categories except for carboxylic acid series are within 15 %. In contrast, the error distribution for carboxylic acids is gathered around 20 % and spreads up to 118 %, which leads to a large error of 29.3 % on average. These results suggest that the dipole moment of carboxylic acids may depend on not only on the –COOH functional group but also other factors which are not included here. However, it is found that for all the functional groups, including carboxylic acids, the ADO rate constants calculated using μ_D(FG) have high accuracies with differences of ≈ 10 % with respect to rate constants that were measured, as discussed in Section 3.3.1. This demonstrates that the dipole moments, as estimated by functional groups, can be used to calculate ADO rate constants.

Although each VOC compound shown in Fig. 3 contains a single functional group, many compounds of interest in the atmosphere have other functional groups and/or multiple groups. In addition, there are cases where the functionality of VOCs detected by PTR-MS cannot be determined. As an alternative, the dipole moments μ_D for such compounds might be estimated from elemental composition HCP_m, denoted as μ_D(HCP_m). The values of μ_D(HCP_m) in individual HCP_m categories, shown in Table 4e, were obtained by averaging μ_D(FG) and $\mu_{D\ meas.}$ for the compounds possessing that HCP_m composition and functional groups except for those used in Fig. 3, which are categorized as “Others” in Table 4b. The accuracy of μ_D(HCP_m) relative to $\mu_{D\ meas.}$ are quite poor compared with that of μ_D(FG). The maximum average error of μ_D(HCP_m) is 160.3 % for the tertiary amine (Table 4h). However, large errors of μ_D(HCP_m) do not necessarily translate into large errors in ADO rate constants. The impact on ADO rate constant from the uncertainties in μ_D(HCP_m) depends on its relative magnitude compared to induced dipole moment as measured by polarizability. The details will be discussed in Section 3.3.1.

If VOCs are detected by PTR-MS with only a quadrupole analyzer, that is, if only nominal mass of VOCs are determined, their elemental composition cannot be determined. In this case, their dipole moments are assumed as a constant value $\mu_D(M_R)$ obtained by averaging μ_D(HCP_m) for

HC (= 0 D), i.e., $\mu_D(M_R)$ = 2.1 ± 0.9 D (Table 4f). The relative errors of $\mu_D(M_R)$ are rather poor compared to those of $\mu_D(HCP_m)$ for almost all the compound categories (i.e., the maximum error is 182.6 % as shown in Table 4i).

3.2.3. Locking constant

The locking constant C in the ADO theory (Eq. 11) is a parameter between 0 and 1 ($0 \leq C \leq 1$) that determines the degree of alignment between the permanent dipole moment of a certain polar compound R with the ionic charge during the ion-molecule collision [13]. Complete alignment of the dipole corresponds to C = 1, no alignment to C = 0. It has been proposed that C is a function of the polarizability α and the permanent dipole moment μ_D of R, i.e., $C = f(\mu_D/\alpha^{1/2})$, at constant temperature [13]. The open circles in Fig. 4a represents the original data points of the locking constant C against $\mu_D/\alpha^{1/2}$ at 300 K reported by Su and Bowers [13]. These data points are well-represented by a log-normal function of $\mu_D/\alpha^{1/2}$ (correlation coefficient r = 0.993):

$$\text{original } C = f(\mu_D/\alpha^{1/2}) = K_0 + K_1\, exp\left\{-\left[\frac{\ln\{(\mu_D/\alpha^{1/2})/K_2\}}{K_3}\right]^2\right\} \qquad (16)$$

K_0 = -0.14 ± 0.08, K_1 = 0.42 ± 0.09, K_2 = 4.2 ± 1.3, K_3 = 3.6 ± 0.7

Su and Bowers calculated the values for the locking constant by substituting the theoretical thermal rate constants in the ADO theory (Eq. 11) for specific values of α and μ_D of various compounds [13]. The theoretical thermal rate constants used in their work [13] were obtained based on the model consisting of a point charge ion interacting with a polar molecule approximated as a two-dimensional rotor, in which only α and μ_D are taken into account as the main factors [43].

(Figure 4)

Here we calculated the ADO rate constants (k_{ADO}) for the proton-transfer reactions between H_3O^+ and 40 polar compounds, using the original locking constant curve (Eq. 16) as well as known values of polarizability ($\alpha_{meas.}$ [20]) and dipole moment ($\mu_{D\ meas.}$ [20]). Red symbols in Fig. 5 show the scatter plot of the resulting ADO rate constants versus the measured ones [16,23,24,26-29]. A linear fit to the data exhibits a slope of 0.75 ± 0.02, an intercept of 0.29 ± 0.06 [x 10^{-9} cm^3 $molecule^{-1}$ s^{-1}], and a correlation coefficient (r) of 0.9886. Relative errors (in %) of ADO rate constants with

respect to measured rate constants were 14.1 % on average. The slope of the best-fit line indicates that for exothermic proton-transfer reactions of H_3O^+, Eq. (16) underestimates the measured values. Su and Bowers remarked that all the proton-transfer reaction rate constants are not accurately described by the ADO theory using the original locking constant data, because of the limitation of the model to obtain the theoretical thermal rate constants [13]. For example, when using original locking constant data, the exothermic proton transfer from *tert*-$C_4H_9^+$ to several amines was calculated to have ADO rate constants that were 1.18-1.54 times higher than measured values [13]. The difference between the ADO and measured rate constants has been explained by the internal energy of the *tert*-$C_4H_9^+$ ion and the nature of ion-molecule collision complex, which are not taken into consideration in the theoretical thermal rate constants and resulting locking constants [44]. In this work, we found that $k_{meas.}$ and k_{ADO} for proton-transfer reactions of H_3O^+ can be corrected only by +0.11-parallel shift of the original locking constant curve along to the *C* axis, which corresponds to $\Delta K_0 = +0.11$ (Fig. 4). Therefore, the modified locking constant curve shown as Fig. 4b is expressed as follows:

$$\text{modified } C = f(\mu_D/\alpha^{1/2}) = modified\ K_0 + K_1\ exp\left\{-\left[\frac{\ln\{(\mu_D/\alpha^{1/2})/K_2\}}{K_3}\right]^2\right\} \qquad (17)$$

modified K_0 = -0.03 ± 0.08, K_1 = 0.42 ± 0.09, K_2 = 4.2 ± 1.3, K_3 = 3.6 ± 0.7

The derivation of Eq. (17) is given in Appendix A.

(Figure 5)

When the modified locking constant curve is applied to ADO theory (Eq. 11), the accuracy of k_{ADO} for proton-transfer reactions of H_3O^+ with respect to measured rate constants significantly improves. The scatter plot of k_{ADO} calculated using the modified locking constant curve (Eq. 17) versus $k_{meas.}$ is shown as blue symbols in Fig. 5. The linear fit exhibits a slope of 1.00 ± 0.01, an intercept of 0.05 ± 0.04 [x 10^{-9} cm^3 $molecule^{-1}$ s^{-1}], and correlation coefficient (*r*) of 0.9957. Relative errors of those k_{ADO} with respect to $k_{meas.}$ are 2.6 % on average.

3.3. Accuracy of ADO rate constant calculated using molecular mass, elemental composition, and functionality

The comparison between measured and ADO rate constants in Fig. 5 is shown for polar compounds with known polarizabilities and dipole moments. These parameters are not known for all compounds of interest, but will be estimated using the methods described above in Sections 3.2.1

and 3.2.2. In this section, we investigate the accuracy of the ADO rate constants for compounds with estimated polarizability and dipole moment, based on molecular mass, elemental composition, and/or functional groups.

3.3.1. Rate constant for polar compounds

Here the ADO rate constants for proton-transfer reactions between H_3O^+ and 81 polar compounds at 300 K were calculated as described in the previous sections using the polarizability estimated from molecular mass and elemental composition ($\alpha(M_R, HCP_m)$) or molecular mass only ($\alpha(M_R)$), the dipole moment from functional group (μ_D(FG)), elemental composition ($\mu_D(HCP_m)$), or molecular mass only ($\mu_D(M_R)$), and the modified locking constant (Eq. 17). The number and chemical properties of the compounds used in each compound category are summarized in Tables 5b and c. Various acronyms for polarizability α and dipole moment μ_D are explained in Scheme 1. Figure 6 shows the comparison of the 3 different ADO rate constants ($k_{ADO}[\alpha(M_R, HCP_m), \mu_D(FG)]$, $k_{ADO}[\alpha(M_R, HCP_m), \mu_D(HCP_m)]$, and $k_{ADO}[\alpha(M_R), \mu_D(M_R)]$) with the measured ones ($k_{meas.}$ [16,23,24,26-29]). The relative errors (in %) of those ADO rate constants with respect to measured values for each compound category are summarized in Tables 5e – g. Table 4d shows the errors for the ADO rate constants calculated using the measured polarizability and dipole moment (blue symbols in Fig. 5). These results suggest that the accuracy of $k_{ADO}[\alpha, \mu_D]$ is strongly dependent on the parameterized dipole moment (i.e., the measured dipole moment, $\mu_{D\ meas.}$ vs. the dipole moment estimated from the functional group, μ_D(FG) vs. the dipole moment estimated from the molecular composition, $\mu_D(HCP_m)$ vs. the dipole moment estimated from the molecular mass only, $\mu_D(M_R)$). The k_{ADO} values estimated from $\mu_{D\ meas.}$ and μ_D(FG) are in good agreement with $k_{meas.}$, fitted by linear functions with slope ≈ 1, intercept ≈ 0, and correlation coefficient (r) ≥ 0.9658 (blue symbols in Fig. 5 and Fig. 6a). The resulting average errors of k_{ADO} relative to $k_{meas.}$ are within 5 %. When only the elemental composition of a compound is known, the agreement between $k_{meas.}$ and k_{ADO} is poor; the best linear fit to the data has slope = 0.20, intercept = 2.3 [x 10^{-9} cm^3 $molecule^{-1}$ s^{-1}], correlation coefficient (r) = 0.38, and the corresponding average error is 19.4 % (Fig. 6b). This disagreement is due to significant deviation of k_{ADO} from $k_{meas.}$ for the categories of ketone/aldehyde, nitrile, primary amine, secondary amine, and tertiary amine. These isobaric compounds have significantly different structures and, consequently, dipole moments, which are poorly represented by their averages. When only the elemental composition of a compound is unknown, the agreement between $k_{meas.}$ and k_{ADO} is further deteriorated and corresponding average error is 24.1 % (Fig. 6c), which results from large errors of $\mu_D(M_R)$ relative to $\mu_{D\ meas.}$ for almost all categories of the compound.

(Figure 6)

It should be noted here that the accuracy of $k_{ADO}[\alpha, \mu_D]$ calculated using the dipole moments estimated from functional group and/or elemental composition, i.e., μ_D(FG) and μ_D(HCP_m), is better than the dipole moments themselves. The maximum relative error of μ_D(FG) with respect to $\mu_{D\ meas.}$ is 29.3 % for the carboxylic acid category (Table 4g). When this μ_D(FG) is used in the ADO theory (Eq. 11), the resulting errors of $k_{ADO}[\alpha(M_R,$ HCP_m), μ_D(FG)] against $k_{meas.}$ are ≈ 7 % (Table 5e). In contrast, $k_{ADO}[\alpha(M_R,$ HCP_m), μ_D(HCP_m)] calculated using μ_D(HCP_m) with maximum error of 160.3 % for the tertiary amine category (Table 4h) have errors of ≈ 50 % (Table 5f). This improvement in accuracy is likely due to the first term in Eq. (11) containing the polarizabilities $\alpha(M_R,$ HCP_m), which is known with a high accuracy related to α_{meas}. Based on these results, if the dipole moment of a polar compound is unknown but its functional group is identified, the ADO rate constant can be obtained with good accuracy (10 % on average). If neither the dipole moment nor the functional group of a compound is known, the estimated dipole moment based on only the elemental composition has a poor accuracy, but the ADO rate constant can still be estimated within 50 %. This accuracy leads to the calculation of sensitivity within 50 % error which is sufficient to address specific science questions.

3.3.2. Rate constant for nonpolar compounds

As described in Section 3.2.2, permanent dipole moments μ_D of nonpolar compounds with elemental composition HC can be approximated as zero in the ADO theory. Therefore, the ADO rate constant between H_3O^+ and a hydrocarbon is calculated using the Langevin theory (Eq. 10). Here, values of k_{ADO} at 300 K for 29 nonpolar compounds were calculated by using two different polarizabilities; $\alpha_{meas.}$ [20] and $\alpha(M_R,$ HCP_m), which are obtained using molecular mass M_R and the linear function $\alpha = 0.142\ M_R - 0.3$ (best fit to the data in Fig. 2a). The resulting rate constants were compared with the previously measured rate constants at 300 K ($k_{meas.}$ [1,21-25,30-34]), as shown in Fig. 7. The number and chemical properties of the compounds used here are summarized in Table 5c. Figure 7 indicates that k_{ADO} calculated using both $\alpha_{meas.}$ and $\alpha(M_R,$ HCP_m) are in good agreement with k_{meas}. A linear regression yields a slope of 0.90 and 0.97, an intercept of 0.2 and 0.1 [x 10^{-9} cm^3 $molecule^{-1}$ s^{-1}], and a correlation coefficient (r) = 0.97 and 0.95, respectively. We exclude (cyclo)alkanes (i.e., methylcyclohexane, cyclooctane, octane and decane) from this calculation. It has been reported that $k_{meas.}$ for proton-transfer reactions between H_3O^+ and alkanes are lower than k_{ADO} due to fragmentation [15,33]. For example, the exothermic proton-transfer reactions of H_3O^+ with methylcyclohexane and cyclooctane involve significant rearrangement resulting in ring-dissociation [33]. The average relative error (in %) of k_{ADO} calculated using $\alpha_{meas.}$ and $\alpha(M_R,$ HCP_m) with respect to $k_{meas.}$ (excluding (cyclo)alkanes) were 6.1 % and 6.5 %, respectively (see Tables 5d and e). These results demonstrate that for nonpolar species, the accuracies of ADO rate constants calculated using measured polarizability versus estimated one in Eq. (10) are similar to within 10 %.

(Figure 7)

When only the nominal mass of a compound is known and its elemental composition cannot be determined, Eq. (10) is not used. The ADO rate constant of such a compound is calculated by substituting polarizability α and dipole moment μ_D estimated from molecular mass only, i.e., $\alpha(M_R)$ = 0.13 M_R – 1.3 (Table 3e) and $\mu_D(M_R)$ = 2.1 D (Table 4f), in Eq. (11). For nonpolar compounds, the resulting ADO rate constants significantly overestimate the measured ones (see green symbols in Fig. 7). This overestimation is due to the value of $\mu_D(M_R)$ being substantially higher than dipole moment of nonpolar species (≈ 0 D). This suggests that the identification of elemental composition by high mass resolution measurement is needed to accurately calculate ADO rate constants.

3.4. Calculation of sensitivity in PTR-MS

The sensitivities of VOCs detected in PTR-MS can be calculated via the following procedures: (i) Determination of the instrument function *Sensitivity* = a x k + b (Eq. 9) using measured sensitivities originating from detected ion intensities and thermal reaction rate constants for a few selected standards. (ii) Substituting measured or ADO rate constants at 300 K for VOCs of interest in Eq. (9). As discussed in 3.1, the standards used to determine Eq. (9) should have small uncertainties of fragmentation and ion transmission efficiencies.

The accuracy of calculated sensitivity relative to measured one is estimated from the uncertainties of the instrument function (Eq. 9) and the rate constant used. When sensitivity is calculated from measured rate constant ($k_{meas.}$), its accuracy is determined by the uncertainties of the coefficients a and b in Eq. (9). The results obtained in Fig. 1 suggest that this accuracy is generally within 15 %. When using ADO rate constant (k_{ADO}), the uncertainty of k_{ADO} against $k_{meas.}$ is involved in the accuracy of sensitivity, as well as the coefficients' uncertainties. Taking into account error propagation, the k_{ADO} using dipole moment measured or estimated from functional group can result in the sensitivities within a 15 % accuracy. The sensitivities calculated using k_{ADO} with dipole moment estimated from elemental composition have the accuracy within 50 %. The k_{ADO} including estimated dipole moment based on molecular mass only leads to sensitivity with accuracy over 50 %. This suggests that if emissions from a mass that has various compounds with different elemental composition but the same nominal molecular mass are measured by high mass resolution instruments, we can at least estimate neutral concentration (in ppbv) of compounds for each elemental composition category within 50 % accuracy. A measurement accuracy of 50 %, where no calibration standard is available, can still be sufficient to answer specific science questions. It should be

noted that the calculation of sensitivity with accuracy described above is valid over the range of minimum and maximum rate constants for the compounds used to obtain the instrument function (Eq. 9).

The overall methodology to calculate the sensitivity in PTR-MS using measured and ADO rate constants are shown in Scheme S-1.

Conclusions

The correlation between sensitivities of VOCs measured by PTR-MS and those calculated from reaction rate constants was investigated. It was found that the sensitivities normalized and corrected for fragmentation and transmission efficiencies of protonated VOCs are well-represented by a linear function of the rate constants measured at 300 K. We also described how polarizability, permanent dipole moment, and ADO rate constant for proton-transfer reaction of H_3O^+ can be estimated for various VOCs, using the information obtained from PTR-MS measurements, i.e., molecular mass, elemental composition, and functionality of VOCs. The results are summarized as follows:

1. The polarizabilities for a given class of compounds can be described within 10 % by a linear function of their molecular masses.
2. The dipole moments for compounds with a specific functional group but different residual hydrocarbon parts, can be approximated within 15 % as a constant value, except for the carboxylic acid series for which the group average has an uncertainty of within 30 %.
3. The locking constants from the literature using simplified ion-molecule collision assumptions lead to 25 % underestimates of the ADO rate constant versus the measured rate constant. Using a modified locking constant, a significantly better agreement between measured and ADO rate constant is obtained.
4. ADO rate constants calculated using polarizability and dipole moment, as estimated from molecular mass, elemental composition, and functional group, as well as the modified locking constant have a high accuracy within 10 % relative to those that were measured.
5. The dipole moments estimated from elemental composition result in the ADO rate constants with accuracies within 50 %. In the case of the ADO rate constants estimated only from molecular mass, the corresponding accuracy is distributed up to 65 %.

In conclusion, the sensitivity of a PTR-MS instrument for many species of interest can be estimated with an accuracy of 15 % from the molecular mass, the elemental composition, and the specific functional groups present, by calibrating the instrument using a few selected standards only. When the functional group of a compound is not known or a compound has more than one functional group, the sensitivity can be estimated with a lower accuracy of 50 %. This suggests that if various VOC isobars are measured by high mass resolution instruments, we can at least estimate the concentrations of neutral VOCs for each elemental composition category within a 50 % accuracy. This accuracy, in the absence of calibration standards, can still be sufficient to answer specific science questions.

Acknowledgments

This work was supported by JSPS postdoctoral Fellowships for Research Abroad and a Grant-in-Aid for Young Scientists (B) (15K16117) from the Ministry of Education, Culture, Sports, Science and Technology of Japan. A. Koss acknowledges the support from the NSF Graduate Fellowship Program. M. Coggon acknowledges the CIRES Visiting Postdoctoral Fellowship. S-M Li acknowledges a CIRES Senior Visiting Fellowship and the support of the Environment and Climate Change Canada's Climate and Clean Air Program (CCAP). K. Sekimoto thanks Yukiumi Kita of Yokohama City University for many helpful suggestions in this work.

Appendix A: Derivation of modified locking constant

It has been shown that the measured rate constants used in Fig. 5 [16,23,24,26-29], which have been obtained by selected ion flow mass spectrometry, are equivalent to the capture rate constants calculated by numerical trajectory parameterization [14]. The assumption of ions and neutral molecules in the model to obtain the capture rate constants, i.e., the approximation as a point charge and two-dimensional rigid rotor respectively [14], is the same assumption employed to calculate the theoretical thermal rate constants [13]. However, unlikely the model of thermal rate constant, the model of the capture rate constants accounts for various factors in addition to polarizability α and dipole moment μ_D, such as angular momentum and moment of inertia of neutral molecule. It has been reported in the trajectory parameterization study [14] that the ratio of the capture rate constants ($k_{capture}$) to the Langevin ones ($k_{Langevin}$) at a constant temperature can be expressed as a function of the single variable $\mu_D/\alpha^{1/2}$, i.e., $k_{capture}/k_{Langevin} = f(\mu_D/\alpha^{1/2})$. This implies that the dependence of the factors other than polarizability α and dipole moment μ_D on the capture rate constants can be parameterized in a function of α and μ_D only. Taking into account the equivalence of the measured rate constants ($k_{meas.}$) used here to the capture rate constants ($k_{capture}$), it can be expected that the ratio of $k_{meas.}$ to $k_{Langevin}$ ($k_{meas.}/k_{Langevin}$) is also shown as a function of $\mu_D/\alpha_{1/2}$. It should be noted here that the variable $\mu_D/\alpha_{1/2}$ is common to the functions expressing the locking constants C in the ADO theory and the ratio of ADO rate constant to $k_{Langevin}$ ($k_{ADO}/k_{Langevin}$) as derived from Eq. (11). This suggests that the difference between $k_{meas.}/k_{Langevin}$ and $k_{ADO}/k_{Langevin}$ (i.e., the difference between $k_{meas.}$ and k_{ADO}) can be corrected by modifying the coefficients $K_0 - K_4$ in the function of the original locking constant curve (Eq. 16).

Figure A-1 shows the ratios of the measured or ADO rate constants with the original locking constant data to the Langevin ones ($k_{meas.}/k_{Langevin}$ or $k_{ADO}/k_{Langevin}$) as a function of $\mu_D/\alpha^{1/2}$ for the 40 compounds used in Section 3.2.3. The Langevin rate constants were calculated by substituting measured polarizability ($\alpha_{meas.}$ [20]) in Eq. (10). Both the ratios $k_{meas.}/k_{Langevin}$ and $k_{ADO}/k_{Langevin}$ are well-fitted by a linear function of $\mu_D/\alpha^{1/2}$:

$$k_{meas.\ or\ ADO}/k_{Langevin} = e \times (\mu_D/\alpha^{1/2}) + f \qquad \text{(A-1)}$$

Interestingly, the principal difference in linear function between $k_{meas.}/k_{Langevin}$ and $k_{ADO}/k_{Langevin}$ is only the slope e (1.55 for $k_{meas.}/k_{Langevin}$ and 1.11 for $k_{ADO}/k_{Langevin}$), whereas the values of the intercept f are almost identical (≈ 0.75). In order to investigate how the coefficients $K_0 - K_4$ in Eq. (16) should be modified to correct only the slope e in Eq. (A-1), the equation of $k_{ADO}/k_{Langevin}$ shown in Eq. (A-2a), obtained by substituting Eq. (16) in Eq. (11), is approximated as a linear function via Taylor expansion. Eq. (A-2b) corresponds to the first approximation equation of $k_{ADO}/k_{Langevin}$, in which the two Taylor series of (i) $exp\left\{-\left[\frac{\ln\{(\mu_D/\alpha^{1/2})/K_2\}}{K_3}\right]^2\right\}$, which is a factor in Eq. (A-2a), and (ii) the intermediate factor $(\mu_D/\alpha^{1/2})\ln(\mu_D/\alpha^{1/2})$ evaluated at the points ϑ and τ, respectively, are used:

$$\frac{k_{ADO}}{k_{Langevin}} = 1 + \left[K_o + K_1\, exp\left\{-\left[\frac{\ln\{(\mu_D/\alpha^{1/2})/K_2\}}{K_3}\right]^2\right\}\right] \times (\mu_D/\alpha^{1/2}) \times (2/\pi k_B T)^{1/2} \qquad \text{(A-2a)}$$

$$\cong (2/\pi k_B T)^{1/2} \times [X(\ln\tau + 1) + Y] \times (\mu_D/\alpha^{1/2}) + \left[1 - (2/\pi k_B T)^{1/2} \times X \times \tau\right] \qquad \text{(A-2b)}$$

$$X = -2\,\vartheta\, K_1\, K_3^{-1} \exp(-\vartheta^2)$$

$$Y = K_0 + K_1 \times \left(1 + 2\vartheta^2 + 2\vartheta K_3^{-1} \ln K_2\right) \times \exp(-\vartheta^2)$$

K_0 = -0.14 ± 0.08, K_1 = 0.42 ± 0.09, K_2 = 4.2 ± 1.3, K_3 = 3.6 ± 0.7

According to Eqs. (A-1) and (A-2b), the slope e and intercept f in Eq. (A-1) correspond to $(2/\pi k_B T)^{1/2}$ x $[X(\ln\tau + 1) + Y]$ and $[1 - (2/\pi k_B T)^{1/2}$ x X x $\tau]$ in Eq. (A-2b), respectively. Here we note that the slope e can be changed only by modifying the coefficient K_0 in the factor Y, and that K_0 modification does not affect the intercept f. Based on Eq. (A-2b) and the values of the slope e obtained in Fig. A-1, modified K_0 can be deduced from the following equations:

$$\text{Modified } K_0 = K_0 + \Delta K_0 = -0.03 \qquad \text{(A-3a)}$$

$$\Delta K_0 = \frac{\Delta slope\ e}{(2/\pi k_B T)^{1/2}} = +0.11 \qquad \text{(A-3b)}$$

$$\Delta \text{ slope } e = \text{slope } e\ (k_{\text{meas.}}/k_{\text{Langevin}}) - \text{slope } e\ (k_{\text{ADO}}/k_{\text{Langevin}}) = +0.44 \qquad \text{(A-3c)}$$

Therefore, the modified locking constant curve is expressed as Eq. (17) in the text.

References

[1] W. Lindinger, A. Hansel, A. Jordan, On-line monitoring of volatile organic compounds at pptv levels by means of proton-transfer-reaction mass spectrometry (PTR-MS): medical applications, food control and environmental research, Int. J. Mass Spectrom. Ion Processes 173 (1998) 191-241.

[2] J. de Gouw, C. Warneke, Measurements of volatile organic compounds in the earth's atmosphere using proton-transfer-reaction mass spectrometry, Mass Spetrom. Rev. 26 (2007) 223-257.

[3] R.S. Blake, P.S. Monks, A.M. Ellis, Proton-transfer reaction mass spectrometry, Chem. Rev. 109 (2009) 861-896.

[4] M. Graus, M. Muller, A. Hansel, High resolution PTR-TOF: Quantification and formula confirmation of VOC in real time, J. Am. Soc. Mass Spectrom. 21 (2010) 1037-1044.

[5] P. Sulzer, E. Hartungen, G. Hanel, S. Feil, K. Winkler, P. Mutschlechner, S. Haidacher, R. Schottkowsky, D. Gunsch, H. Seehauser, M. Striednig, S. Jürschik, K. Breiev, M. Lanza, J. Herbig, L. Märk, T.D. Märk, A. Jordan, A proton transfer reaction-quadrupole interface time-of-flight mass spectrometer (PTR-QiTOF): High speed due to extreme sensitivity, Int. J. Mass Spectrom. 368 (2014) 1-5.

[6] C. Warneke, P.R. Veres, S.M. Murphy, J. Soltis, R. Field, M.G. Graus, A. Koss, S.-M. Li, R. Li, B. Yuan, J.M. Robert, J.A. de Gouw, PTR-QMS vs. PTR-TOF comparison in a region with oil and natural gas extraction industry in the Uintah Basin in 2013, Atmos. Meas. Tech. 8 (2015) 411-420.

[7] B. Yuan, A. Koss, C. Warneke, J.B. Gilman, B.M. Lerner, H. Stark, J.A. de Gouw, A high-resolution time-of-flight chemical ionization mass spectrometer utilizing hydronium ions (H_3O^+ ToF-CIMS) for measurements of volatile organic compounds in the atmosphere, Atmos. Meas. Tech. 9 (2016) 2735-2752.

[8] J. Herbig, M. Müller, S. Schallhart, T. Titzmann, M. Graus, A. Hansel, On-line breath analysis with PTR-TOF, J. Breath Res. 3 (2009) 027004.

[9] F. Biasioli, F. Gasperi, C. Yeretzian, T.D. Märk, PTR-MS monitoring of VOCs and BVOCs in food science and technology, Trends Anal. Chem. 30 (2011) 968-977.

[10] C. Soukoulis, L. Cappellin, E. Aprea, F. Costa, R. Viola, T.D. Märk, F. Gasperi, F. Biasioli, PTR-ToF-MS, a novel, rapid, high sensitivity and non-invasive tool to monitor volatile compounds release during fruit post-harvest storage: The case study of apple ripening, Food Bioprocess Tech. 6 (2013) 2831-2843.

[11] NIST Chemistry WebBook, 2016, http;//webbook.nist.gov/chemistry/ (last accessed March 2016).

[12] A.H. Goldstein and I.E. Galbally, Known and unexplored organic constituents in the Earth's atmosphere, Environ. Sci. Technol. 41 (2007) 1514–1521.

[13] T. Su, M.T. Bowers, Ion-polar molecule collision: the effect of ion size on ion-polar molecule rate constants; the parameterization of the average-dipole-orientation theory, Int. J. Mass Spectrom. Ion Physics, 12 (1973) 347-356.

[14] T. Su, W.J. Chesnavich, Parameterization of the ion-polar molecule collision rate constant by trajectory calculations, J. Chem. Phys. 76 (1982) 5183-5185.

[15] J. Zhao, R. Zhang, Proton transfer reaction rate constants between hydronium ion (H_3O^+) and volatile organic compounds, Atmos. Environ. 38 (2004) 2177-2185.

[16] L. Cappellin, M. Probst, J. Limtrakul, F. Biasioli, E. Schuhfried, C. Soukoulis, T.D. Märk, F. Gasperi, Proton transfer reaction rate coefficients between H_3O^+ and some sulphur compounds, Int. J. Mass Spectrom. 295 (2010) 43-48.

[17] C. Warneke, J. de Gouw, P. Goldan, R. Fall, Validation of atmospheric VOC measurements by proton-transfer-reaction mass spectrometry using a gas-chromatographic presentation method. Environ. Sci. Technol. 37 (2003) 2494-2501.

[18] J. de Gouw, C. Warneke, T. Karl, G. Eerdekens, C. van der Veen, R. Fall, Sensitivity and specificity of atmospheric trace gas detection by proton-transfer-reaction mass spectrometry, Int. J. Mass Spectrom. 223-224 (2003) 365-382.

[19] A.R. Koss, C. Warneke, B. Yuan, M.M. Coggon, P.R. Veres, J.A. de Gouw, Evaluation of NO^+ reagent ion chemistry for on-line measurements of atmospheric volatile organic compounds, Atmos. Meas. Tech. 9 (2016) 2909-2925.

[20] W.M. Haynes, CRC Handbook of Chemistry and Physics, 2013-2014, 94th Ed. pp. 9-51 and 10-187.

[21] D.B. Milligan, P.F. Wilson, C.G. Freeman, M. Meot-Ner, M.J. McEwan, Dissociation proton transfer reactions of H_3^+, N_2H^+, and H_3O^+ with acyclic, cyclic, and aromatic hydrocarbons and nitrogen compounds, and astrochemical implications, J. Phys. Chem. A 106 (2002) 9745-9755.

[22] F.C. Fehsenfeld, I. Dotan, D.L. Albritton, C.J. Howard, E.E. Ferguson, Stratospheric positive-ion chemistry of formaldehyde and methanol, J. Gyophys. Res. Oceans and Atmospheres 83 (1978) 1333-1336.

[23] P. Spanel, D. Smith, SIFT studies of the reactions of H_3O^+, NO^+ and O_2^+ with a series of volatile carboxylic acids and ester. Int. J. Mass Spectrom. Ion Processes 172 (1998) 137-147.

[24] P. Spanel, D. Smith, Selected ion flow tube studies of the reactions of H_3O^+, NO^+, and O_2^+ with some organosulphur molecules, Int. J. Mass Spectrom. 176 (1998) 167-176.

[25] P. Spanel, D. Smith, Selected ion flow tube studies of the reactions of H_3O^+, NO^+, and O_2^+ with several aromatic and aliphatic hydrocarbons, Int. J. Mass Spectrom. 181 (1998) 1-10.

[26] P. Spanel, Y. Ji, D. Smith, SIFT studies of the reactions of H_3O^+, NO^+ and O_2^+ with a series of aldehydes and ketones, Int. J. Mass Spectrom. Ion Proceses 165/166 (1997) 25-37.

[27] P. Spanel, D. Smith, SIFT studies of the reactions of H_3O^+, NO^+ and O_2^+ with a series of alcohols, Int. J. Mass Spectrom. Ion Processes 167/168 (1997) 375-388.

[28] P. Spanel, D. Smith, Selected ion flow tube studies of the reactions of H_3O^+, NO^+ and O_2^+ with several amines and some other nitrogen-containing molecules, Int. J. Mass Spectrom. 176 (1998) 203-211.

[29] P. Spanel, D. Smith, SIFT studies of the reactions of H_3O^+, NO^+ and O_2^+ with several ethers, Int. J. Mass Spectrom. Ion Processes 172 (1998) 239-247.

[30] P. Spanel, M. Pavlik, D. Smith, Reactions of H_3O^+ and OH^- ions with some organic molecules: applications to trace gas analysis in air, Int. J. Mass Spectrom. Ion Processes 145 (1995) 177-186.

[31] A.M. Diskin, T. Wang, D. Smith, P. Spanel, A selected ion flow tube (SIFT), study of the reactions of H_3O^+, NO^+ and O_2^+ ions with a series of alkenes in support of SIFT-MS, Int. J. Mass Spectrom. 218 (2002) 87-101.

[32] A.J. Midey, S. Williams, S.T. Arnold, A.A. Viggiano, Reactions of $H_3O^+(H_2O)_{0,1}$ with alkylbenzenes from 298 to 1200 K, J. Phys. Chem. A 106 (2002) 11726-11738.

[33] A.J. Midey, S. Williams, T.M. Miller, A.A. Viggiano, Reactions of O_2^+, NO^+ and H_3O^+ with methylcyclohexane (C_7H_{14}) and cyclooctane (C_8H_{16}) from 298 to 700 K, Int. J. Mass Spectrom. 222 (2003) 413-430.

[34] A. Tani, S. Hayward, C.N. Hewitt, Measurement of monoterpenes and related compounds by proton transfer reaction-mass spectrometry (PTR-MS), Int. J. Mass Spectrom. 223/224 (2003) 561-578.

[35] L. Keck, U. Oeh, C. Hoeschen, Corrected equation for the concentrations in the drift tube of a proton transfer reaction-mass spectrometry (PTR-MS), Int. J. Mass Spectrom. 264 (2007) 92-95.

[36] H.R. Shamlouei, M. Tabrizchi, Transmission of different ions through a drift tube, Int. J. Mass Spectrom. 273 (2008) 78-83.

[37] I.V. Chernushevich, A.V. Loboda, B.A. Thomson, An introduction to quadrupole-time-of-flight mass spectrometry, J. Mass Spectrom. 36 (2001) 849-865.

[38] I. Dotan, D.L. Albritton, W. Lindinger, M. Paul, Mobilities of CO_2^+, N_2H^+, H_3O^+, $H_3O^+ \cdot H_2O$, and $H_3O^+ \cdot (H_2O)_2$ ions in N_2, J. Chem. Phys. 65 (1976) 5028-5030.

[39] G.H. Wannier, On the motion of gaseous ions in a strong electric field. I, Phys. Rev. 83 (1951) 281.

[40] A.A. Viggiano, R.A. Morris, J.F. Paulson, Rotational temperature dependences of gas phase ion-molecule reactions, J. Chem. Phys. 89 (1988) 4848-4852.

[41] P. Langevin, A fundamental formula of kinetic theory, Ann. Chim. Phys. 5 (1905) 245.

[42] P.B. Armentrout, Fundamentals of ion-molecule chemistry, J. Anal. At. Spectrom. 19 (2004) 571-580.

[43] T. Su, M.T. Bowers, Theory of ion-polar molecule collisions. Comparison with experimental charge transfer reactions of rare gas ions to geometric isomers of difluorobenzene and dichloroethylene, J. Chem. Phys. 58 (1973) 3027-3037.

[44] T. Su, M.T. Bowers, Ion-polar molecule collisions. Proton transfer reactions of $C_4H_9^+$ ions with NH_3, CH_3NH_2, $(C_2H_5)_2NH$, and $(CH_3)_3N$, J. Am. Chem. Soc. 95 (1973) 7611-7613.

Legends of Tables, Schemes, and Figures

Figure 1. Corrected sensitivities (Table 2b-II) plotted as a function of measured rate constants (Table 2d) for proton transfer reactions of H_3O^+ at 300 K for 11 different VOCs in (a) the H_3O^+-ToF-CIMS, (b) the modified H_3O^+-ToF-CIMS, and (c) the PTR-QMS. Error bars show the uncertainty of the experimental calibration (20 %). The solid line and corresponding equation in each figure are the fit to the data for the VOCs except for methanol. N in each figure describes the number of compounds used.

Figure 2. Literature values of polarizability ($\alpha_{\text{literature}}$) plotted as a function of molecular mass (M_R) for various compounds in the HCP_m categories of (a) HC, (b) HCO_1, (c) HCO_2, (d) $HCO_{3 \text{ or } 4}$, (e) HCN_1, (f) HCN_2, (g) HCN_pO_q (p = 1, 2, 4 and q = 1-4, 8), and (h) HCS_1, along with a best fit to the data (solid line). (i) Structures of the compounds represented as the filled data points in (a), (d), (e), (f) and (g), whose polarizabilities are deviated from those of other compounds. The units of $\alpha_{\text{literature}}$ and M_R used here, [x 10^{-24} cm^3] and [Da], correspond to [x 10^{-30} m^3] and [x 10^{-3} kg mol^{-1}], respectively. N in (a) – (h) in each figure represents the number of compounds used.

Figure 3. The measured permanent dipole moments ($\mu_{D \text{ meas.}}$) plotted as a function of molecular mass (M_R) for various compounds in the HCP_m categories of (a) HCO_1, (b) HCO_2, (c) HCN_1, (d) HCN_1O_q (q = 1 and 2), and (e) HCS_1, along with best constant fits to the data (solid lines). (f) Structures of the compounds represented as the filled data points in (a), (b), (c) and (e), which are deviated from the constant fitting. N in (a) – (e) represents the number of compounds used.

Figure 4. (a) Original data points of the locking constant C against $\mu_D/\alpha^{1/2}$ at 300 K reported by Su and Bowers [13] (open circles) and corresponding fitting curve using a log normal function (Eq. 16). (b) Modified locking constant curve according to Eq. (17). N in each figure represents the number of compounds used. The detailed information of the individual compounds used here is summarized in Table S-3.

Figure 5. Scatter plots of ADO rate constants calculated using the original and modified locking constants C versus measured ones ($k_{\text{meas.}}$) for 40 different polar compounds, along with best fits to the data (solid lines). s, i, and r represent the slope, intercept, and corresponding correlation coefficient for the linear line of the best fit, respectively. $RE_{\text{ave.}}$ is the average value of the relative errors of k_{ADO} relative to k_{meas}. The detailed information of the individual compounds used here is summarized in Table S-3.

Figure 6. Scatter plots of ADO rate constants ($k_{ADO}[\alpha, \mu_D]$) calculated using (a) $[\alpha, \mu_D] = [\alpha(M_R, HCP_m), \mu_D(FG)]$, (b) $[\alpha(M_R, HCP_m), \mu_D(HCP_m)]$, and (c) $[\alpha(M_R), \mu_D(M_R)]$ versus measured ones ($k_{meas.}$) for various polar compounds, along with best fits to the data (solid lines). s, i, and *r* represent the slope, intercept, and corresponding correlation coefficient for the linear line of the best fit, respectively. N in each figure describes the number of compounds used. Error value in each figure corresponds to the average error of $k_{ADO}[\alpha, \mu_D]$ for overall polar compounds shown in Tables 5e – g.

Figure 7. Scatter plots of 3 different ADO rate constants ($k_{ADO}[\alpha_{meas.}]$, $k_{ADO}[\alpha(M_R, HCP_m)]$, and $k_{ADO}[\alpha(M_R), \mu_D(M_R)]$) versus measured ones ($k_{meas.}$) for various nonpolar compounds, along with best fits to the data (solid lines). s, i, and *r* represent the slope, intercept, and corresponding correlation coefficient for the linear line of the best fit, respectively. $RE_{ave.}$ is the average value of the relative errors of k_{ADO} relative to $k_{meas.}$ in individual rate constant categories. N describes the number of compounds used.

Scheme 1. Diagram of how to obtain the values of polarizability, dipole moment, reaction rate constant, and sensitivity in PTR-MS in this study.

Figure A-1. Ratio of the measured rate constants ($k_{meas.}$) or ADO rate constants using the original locking constant (k_{ADO}) to the Langevin ones ($k_{Langevin}$) as a function of $\mu_D/\alpha^{1/2}$ for the 40 compounds used in Section 3.2.3. Solid lines are best fits to the data. N in each figure represents the number of compounds used. The detailed information of the individual compounds used here is summarized in Table S-3.

Table 1. (a) Instrument conditions and (b) functions for the H_3O^+-ToF-CIMS, the modified H_3O^+-ToF-CIMS, and the PTR-QMS.

Table 2. (a) The detailed information of the 11 different volatile organic compounds (VOCs) used to investigate the correlation between the measured sensitivities and reaction rate constants shown in Fig. 1. (b) Sensitivities of the VOCs for the 3 different instruments. (c) Product ion distribution originating from the individual protonated VOCs ($VOC{\cdot}H^+$). (d) Measured rate constants for proton transfer reactions between H_3O^+ and the VOCs at 300 K.

Table 3. (a) Elemental composition categories, (b) total numbers and the molecular mass (M_R) range and (c) chemical class of the compounds R used to investigate the correlation with the literature values of polarizability and number of compounds used in each class shown in Fig. 2. (d) Linear functions fitting between the averages of literature polarizability values ($\alpha_{literature}$) and M_R in individual HCP_m categories and

corresponding correlation coefficients and exceptions. (e) Linear function to obtain $\alpha(M_R)$. Average relative errors of (f) $\alpha(M_R, HCP_m)$ and (g) $\alpha(M_R)$ with respect to those previously measured ($\alpha_{meas.}$). The more detailed information of the individual compounds used here is summarized in Table S-1. Distributions of the relative errors for individual composition categories are shown in Figs. S-1 and S-2.

Table 4. (a) Elemental composition categories, (b) functional groups and molecular mass (M_R) range and (c) chemical properties of residual hydrocarbon part consisting of the compounds R, which were used to investigate the correlation between the measured dipole moments ($\mu_{D\ meas.}$) and number of compounds in each class shown in Fig. 3. (d) Average values of $\mu_{D\ meas.}$ for R in the individual functional group series, $\mu_D(FG)$. (e) Average values of $\mu_D(FG)$ and $\mu_{D\ meas.}$(Others) in the individual HCP_m categories, $\mu_D(HCP_m)$. (f) Average value of $\mu_D(HCP_m)$, $\mu_D(M_R)$. Average relative errors of (f) $\mu_D(FG)$, (g) $\mu_D(HCP_m)$, and (h) $\mu_D(M_R)$ with respect to $\mu_{D\ meas}$. The more detailed information of the individual compounds used here is summarized in Table S-2. Distributions of the relative errors for individual composition categories are shown in Figs. S-3 – S-5.

Table 5. (a) Elemental composition categories, (b) functional groups and (c) chemical properties of residual hydrocarbon part consisting of the compounds R, whose measured rate constants were used in Figs. 6 and 7. (d)-(g) Average relative errors of 4 different ADO rate constants ($k_{ADO}[\alpha, \mu_D]$) with respect to the measured ones ($k_{meas.}$). The more detailed information of the individual compounds used here is summarized in Tables S-4 and S-5. Distributions of the relative errors summarized in (d)-(g) are shown in Fig. S-6.

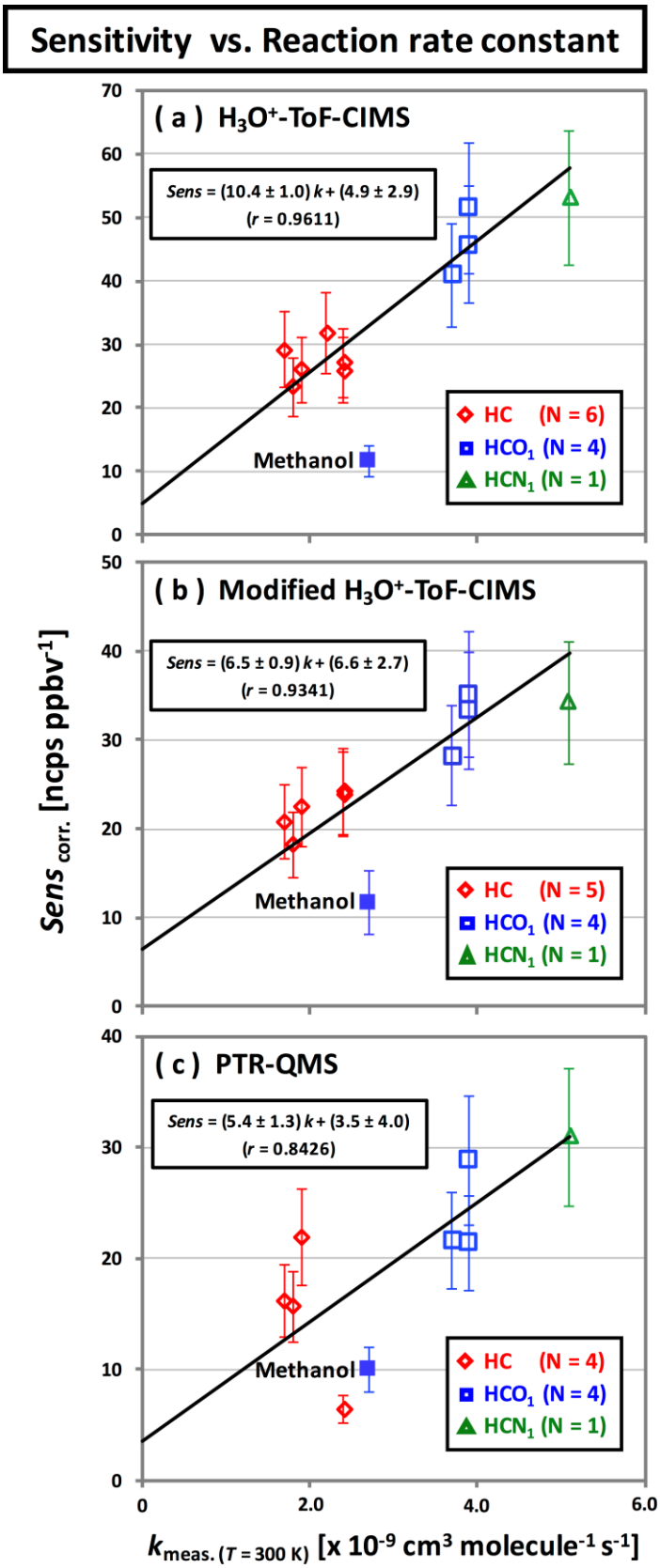

Figure 1. Corrected sensitivities (Table 2b-II) plotted as a function of measured rate constants (Table 2d) for proton transfer reactions of H_3O^+ at 300 K for 11 different VOCs in (a) the H_3O^+-ToF-CIMS, (b) the modified H_3O^+-ToF-CIMS, and (c) the PTR-QMS. Error bars show the uncertainty of the experimental calibration (20 %). The solid line and corresponding equation in each figure are the fit to the data for the VOCs except for methanol. N in each figure describes the number of compounds used.

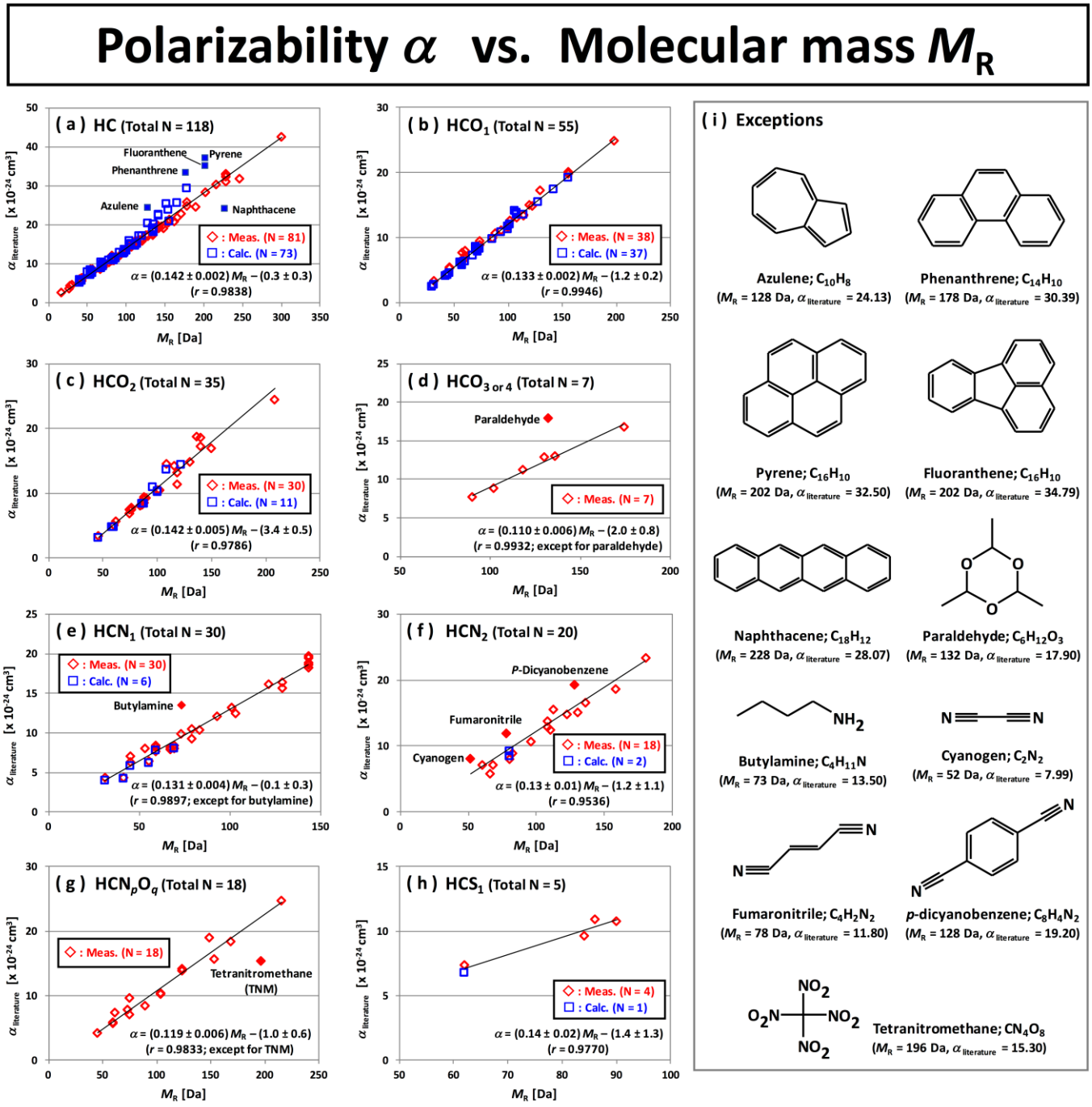

Figure 2. Literature values of polarizability ($\alpha_{literature}$) plotted as a function of molecular mass (M_R) for various compounds in the HCP_m categories of (a) HC, (b) HCO_1, (c) HCO_2, (d) $HCO_{3\ or\ 4}$, (e) HCN_1, (f) HCN_2, (g) HCN_pO_q (p = 1, 2, 4 and q = 1-4, 8), and (h) HCS_1, along with a best fit to the data (solid line). (i) Structures of the compounds represented as the filled data points in (a), (d), (e), (f) and (g), whose polarizabilities are deviated from those of other compounds. The units of $\alpha_{literature}$ and M_R used here, [x 10^{-24} cm^3] and [Da], correspond to [x 10^{-30} m^3] and [x 10^{-3} kg mol^{-1}], respectively. N in (a) – (h) in each figure represents the number of compounds used.

Permanent dipole moment μ_D vs. Molecular mass M_R

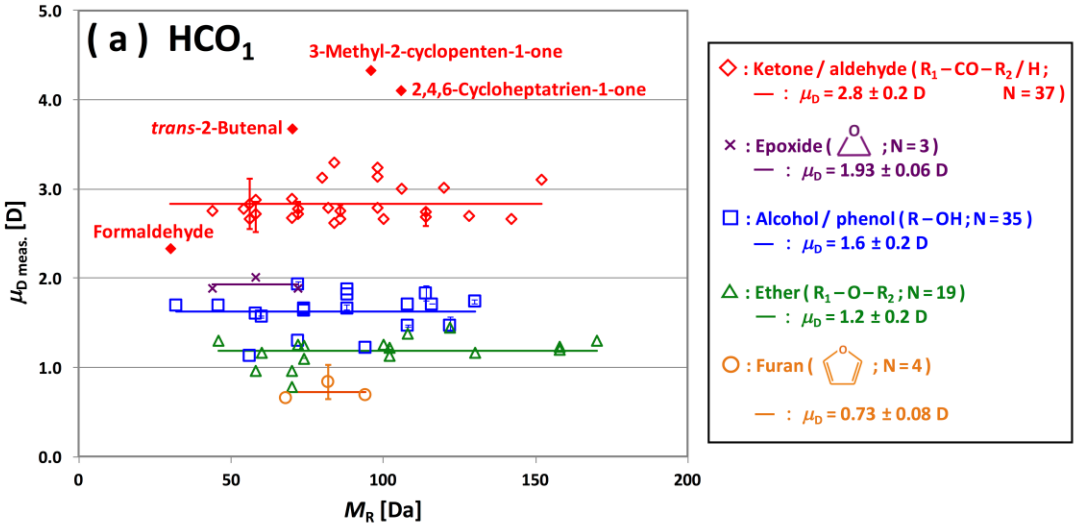

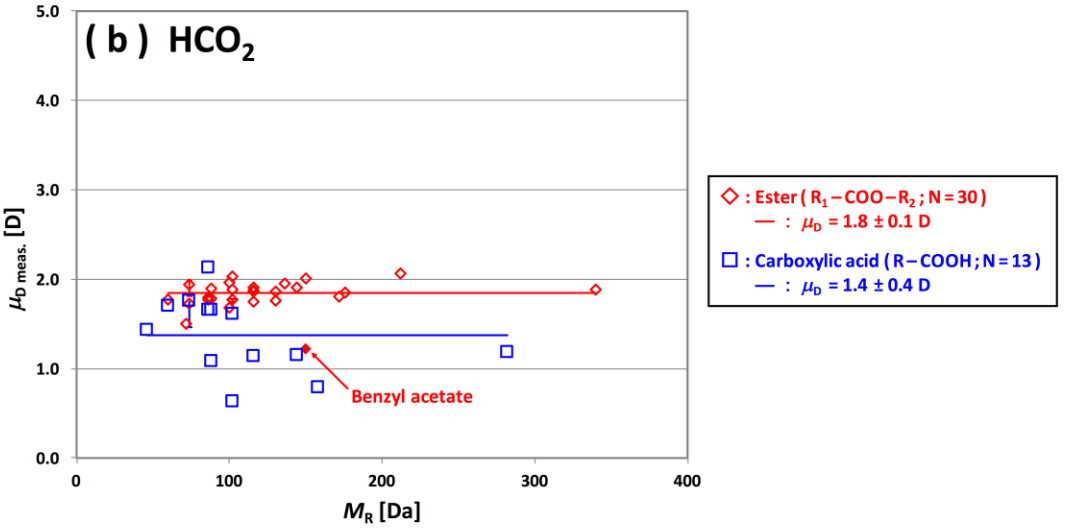

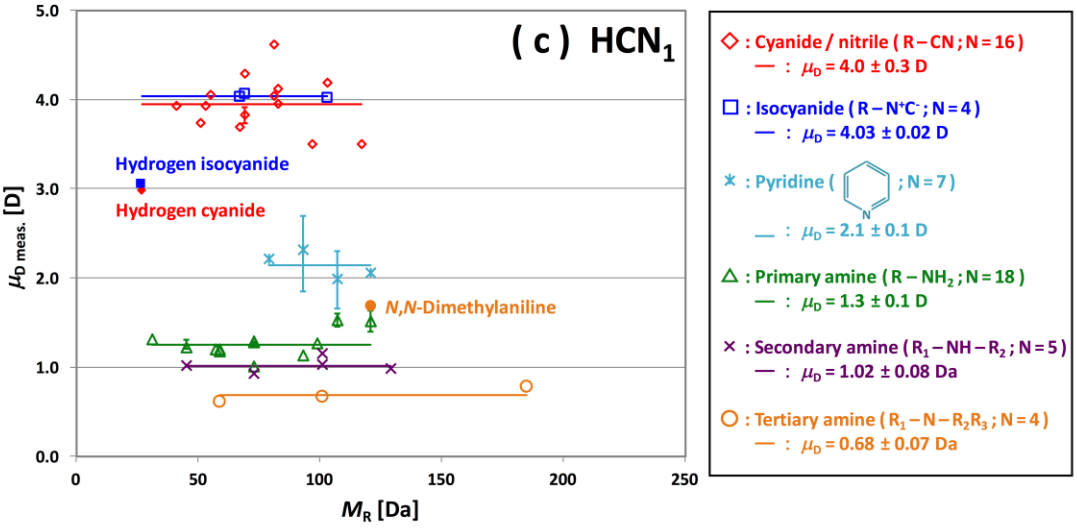

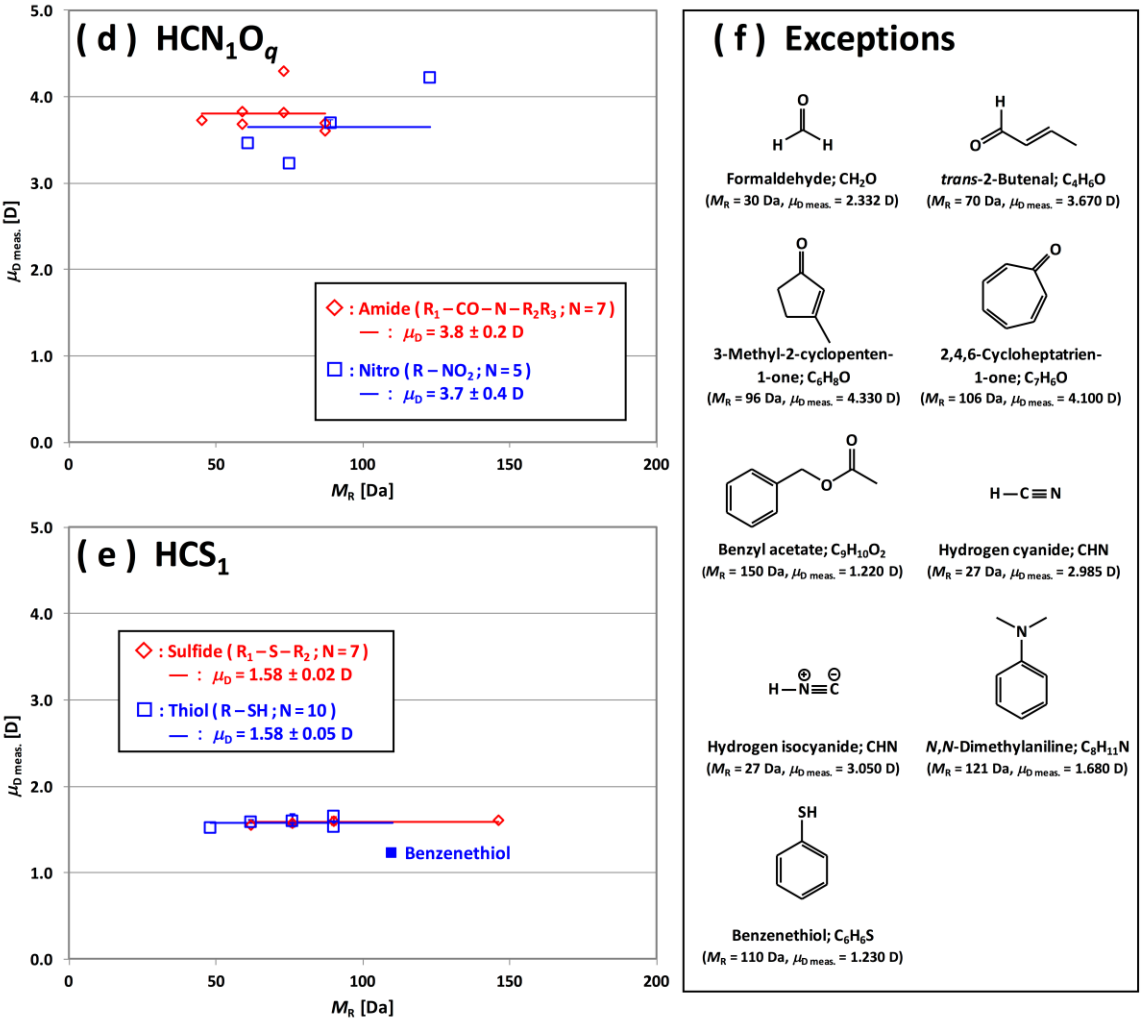

Figure 3. The measured permanent dipole moments ($\mu_{D\ meas.}$) plotted as a function of molecular mass (M_R) for various compounds in the HCP_m categories of (a) HCO_1, (b) HCO_2, (c) HCN_1, (d) HCN_1O_q (q = 1 and 2), and (e) HCS_1, along with best constant fits to the data (solid lines). (f) Structures of the compounds represented as the filled data points in (a), (b), (c) and (e), which are deviated from the constant fitting. N in (a) – (e) represents the number of compounds used.

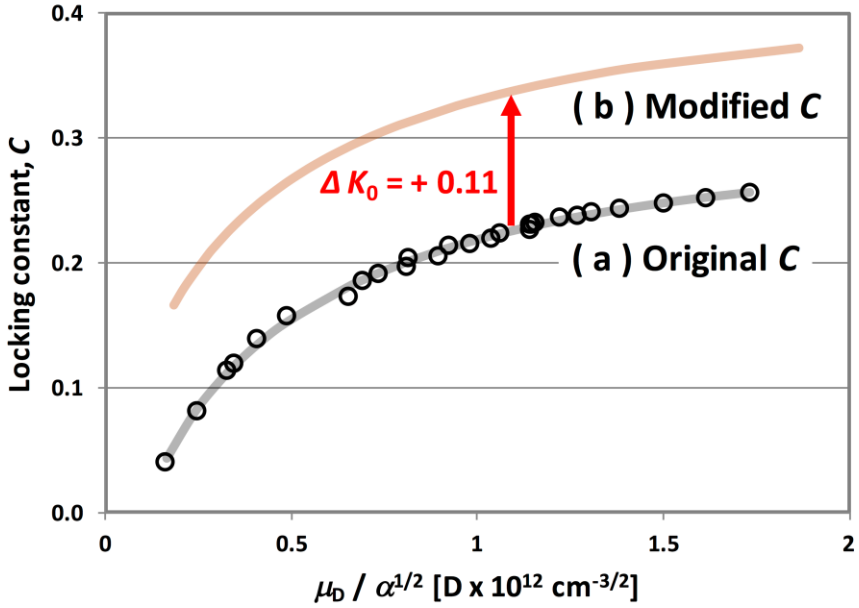

Figure 4. (a) Original data points of the locking constant *C* against $\mu_D/\alpha^{1/2}$ at 300 K reported by Su and Bowers [13] (open circles) and corresponding fitting curve using a log normal function (Eq. 16). (b) Modified locking constant curve according to Eq. (17). N in each figure represents the number of compounds used. The detailed information of the individual compounds used here is summarized in Table S-3.

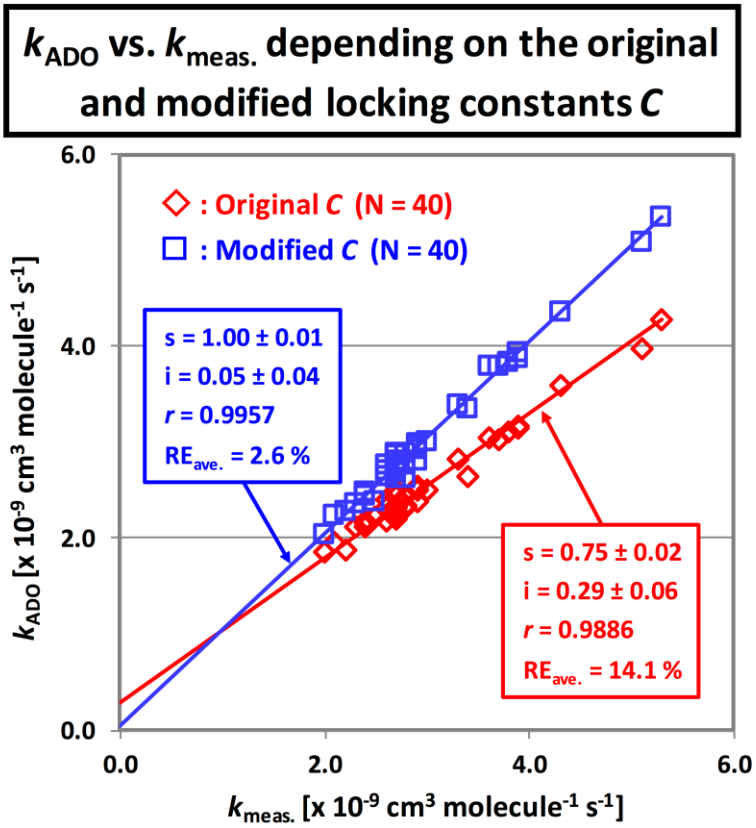

Figure 5. Scatter plots of ADO rate constants (k_{ADO}) calculated using the original and modified locking constants *C* versus measured ones ($k_{meas.}$) for 40 different polar compounds, along with best fits to the data (solid lines). s, i, and *r* represent the slope, intercept, and corresponding correlation coefficient for the linear line of the best fit, respectively. $RE_{ave.}$ is the average value of the relative errors of k_{ADO} relative to k_{meas}. N describes the number of compounds used. The detailed information of the individual compounds used here is summarized in Table S-3.

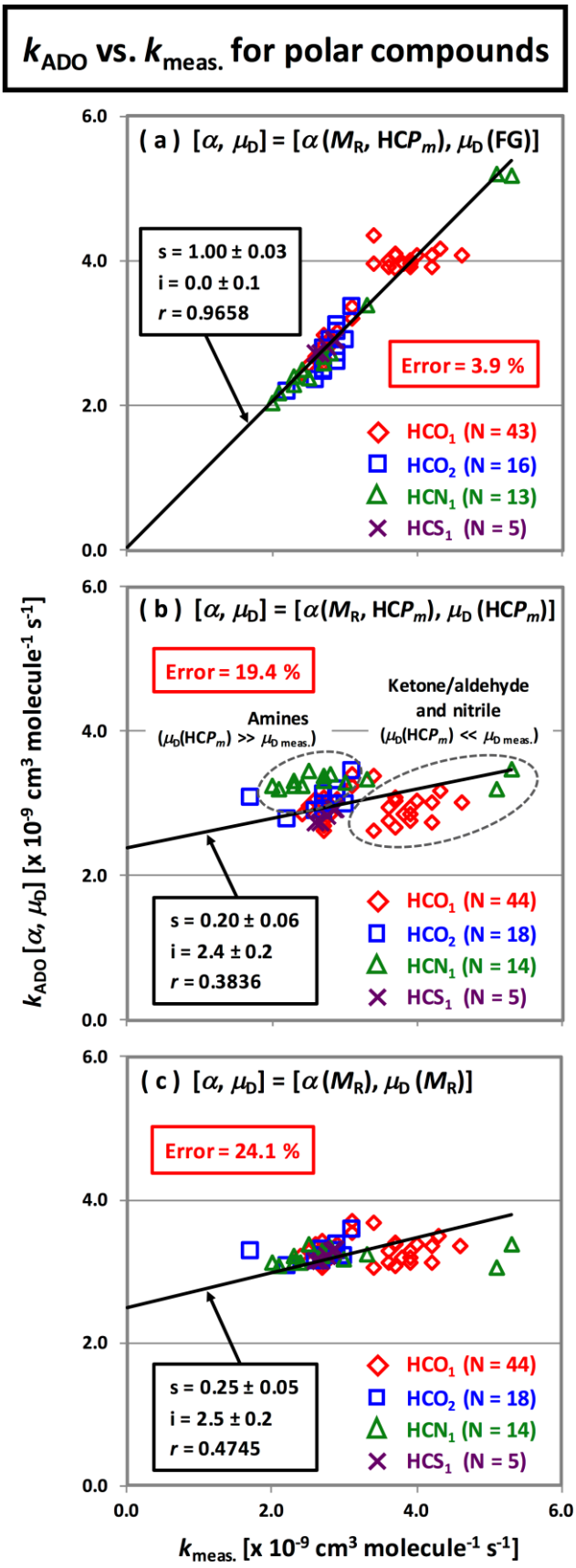

Figure 6. Scatter plots of ADO rate constants (k_{ADO}[α, μ_D]) calculated using (a) [α, μ_D] = [α(M_R, HCP_m), μ_D(FG)], (b) [α(M_R, HCP_m), μ_D(HCP_m)], and (c) [α(M_R), μ_D(M_R)] versus measured ones ($k_{meas.}$) for various polar compounds, along with best fits to the data (solid lines). s, i, and *r* represent the slope, intercept, and corresponding correlation coefficient for the linear line of the best fit, respectively. N in each figure describes the number of compounds used. Error value in each figure corresponds to the average error of k_{ADO}[α, μ_D] for overall polar compounds shown in Tables 5e – g.

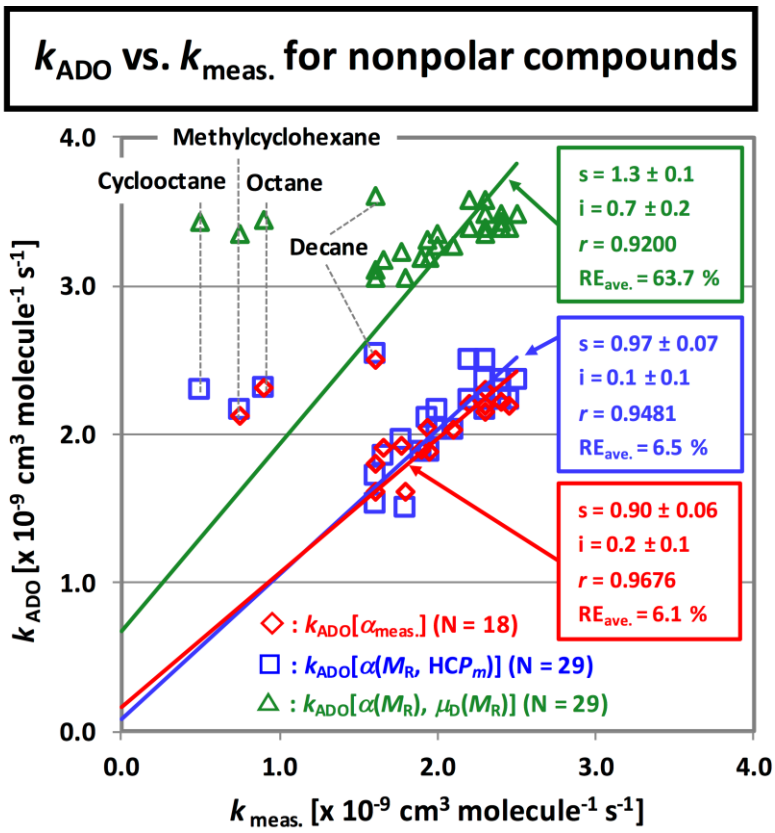

Figure 7. Scatter plots of 3 different ADO rate constants ($k_{ADO}[\alpha_{meas.}]$, $k_{ADO}[\alpha(M_R, HCP_m)]$, and $k_{ADO}[\alpha(M_R), \mu_D(M_R)]$) versus measured ones ($k_{meas.}$) for various nonpolar compounds, along with best fits to the data (solid lines). s, i, and *r* represent the slope, intercept, and corresponding correlation coefficient for the linear line of the best fit, respectively. $RE_{ave.}$ is the average value of the relative errors of k_{ADO} relative to $k_{meas.}$ in individual rate constant categories. N describes the number of compounds used.

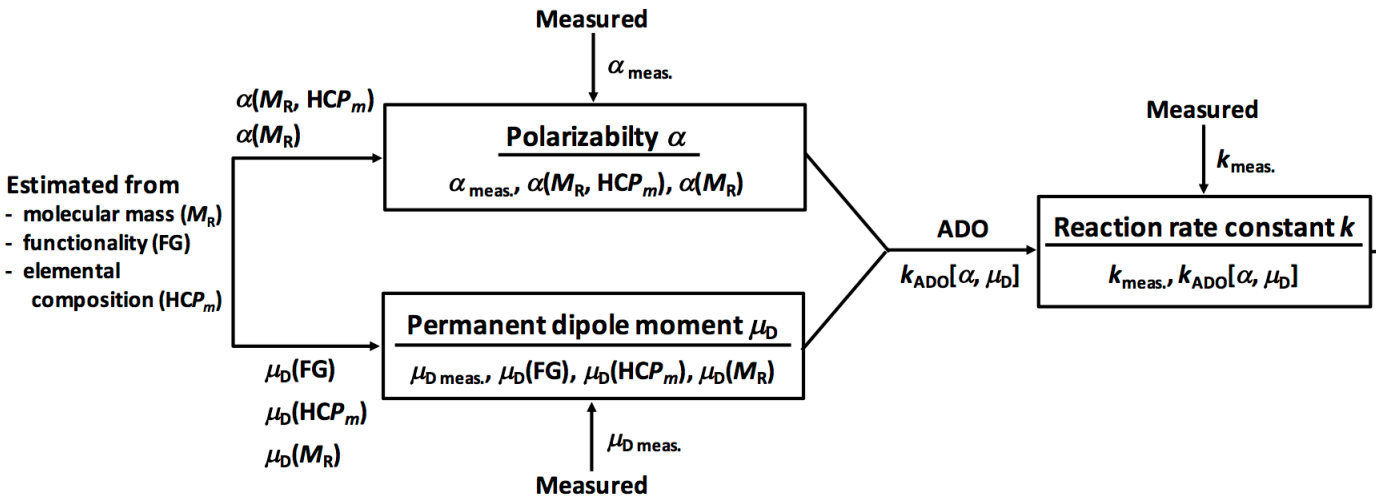

Scheme 1. Diagram of how to obtain the values of polarizability, dipole moment, reaction rate constant, and sensitivity in PTR-MS in this study.

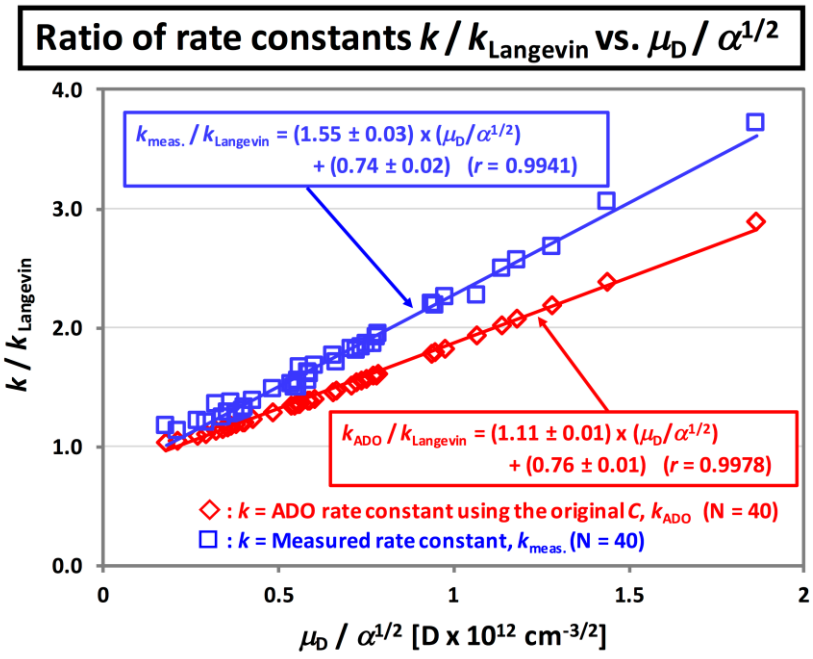

Figure A-1. Ratio of the measured rate constants ($k_{meas.}$) or ADO rate constants using the original locking constant (k_{ADO}) to the Langevin ones ($k_{Langevin}$) as a function of $\mu_D/\alpha^{1/2}$ for the 40 compounds used in Section 3.2.3. Solid lines are best fits to the data. N in each figure represents the number of compounds used. The detailed information of the individual compounds used here is summarized in Table S-3.

Table 1

Instrumentation

				H_3O^+-ToF-CIMS [7]	Modified H_3O^+-ToF-CIMS	PTR-QMS [27,28]
(a) Instrument condition	Drift tube condition	Length	[cm]	11.0	11.0	9.6
		Pressure	[mbar]	2.4	2.4	2.4
		Temperature	[K]	323	323	323
		Voltage	[V]	710	715	547
		E/N ratio	[Td] [a]	120	120	106
	H_3O^+ intensity, I_{H3O+}		[cps]	2.5 x 10^6	9.0 x 10^6	4 .0 x 10^6
	Ion transmission efficiency, $T_{H3O+}/T_{VOC\cdot H+}$			$\sqrt{\frac{m/z_{reference}}{m/z_{VOC\cdot H^+}}} \times 0.14$ [b]	$\sqrt{\frac{m/z_{reference}}{m/z_{VOC\cdot H^+}}} \times 0.32$ [b]	0.63
(b) Instrument function	Linear function: *Sensitivity* = *a k* + *b*			*Sens* = (13.8 ± 0.5) $k_{kinetic}$	*Sens* = (9.0 ± 0.2) $k_{kinetic}$	*Sens* = (7.4 ± 0.6) $k_{kinetic}$
	Factor *A*	[x 10^9 molecule s cm^{-3}]		6.7	6.7	6.6
	Error (slope *a* vs. factor *A*)			107.5 %	35.1 %	10.6 %

a 1 Td = 10-17 V cm2

b The first factor, (m/zreference / m/z VOC・H +)1 /2 , is related to the correction for ToF duty cycle effect, which corresponds to the transmission efficiency of the analyze.

The duty-cycle correction accounts for differences in ion residence time in the extraction region of the ToF and eliminates one mass-dependence of the sensitivity [47].

m/zreference is an arbotrary reference mass (in this study, m/zreference = 55).

The second factor, 0.14 or 0.32, corresponds to the extraction efficiency from the drift tube into the analyer and the detection efficiency.

Table 2.1

Measured sensitivity in PTR-MS vs. kinetic reaction rate constant

(a) Volatile organic compound (VOC)								(b) Sensitivity [ncps ppbv^{-1}]					
								(I) Meausred, $Sens_{meas.}$ [a]			(II) Corrected, $Sens_{corr.}$ [b]		
	HCP_m		Formula	Molecular mass M_R [Da]	Functional group / chemical group	Proton affinity [kJ mol^{-1}] [11]	Vapor pressure [°C at 100 kPa] [30]	H_3O^+-ToF-CIMS	Modified H_3O^+-ToF-CIMS	PTR-QMS [27]	H_3O^+-ToF-CIMS	Modified H_3O^+-ToF-CIMS	PTR-QMS
Polar compound	HCO_1	Methanol	CH_4O	32	Alcohol / phenol	754.3	64.2	63.2 [c]	27.7	15.9	11.6	12.7	9.9
		Acetaldehyde	C_2H_4O	44	Ketone / aldehyde	768.5	20.0	261.6 [c]	89.0	34.5	40.9	31.8	21.6
		Ethanol	C_2H_6O	46	Alcohol / phenol	776.4	78.0	12.8	-	3.0	2.1	-	3.8
		Acrolein	C_3H_4O	56	Ketone / aldehyde	797.0	52.8	-	39.4	-	-	12.9	-
		Acetone	C_3H_6O	58	Ketone / aldehyde	812.0	55.7	366.4 [c]	95.3	41.5	51.5	30.6	28.8
		Methyl ethyl ketone (MEK)	C_4H_8O	72	Ketone / aldehyde	827.3	79.2	354.4 [c]	97.1	34.1	45.7	28.6	21.3
		Anisole	C_7H_8O	108	Ether	839.6	153.2	-	37.9	-	-	9.0	-
	HCO_2	Formic acid	CH_2O_2	46	Carboxylic acid	742.0	100.2	62.8	-	-	9.8	-	-
		Acetic acid	$C_2H_4O_2$	60	Carboxylic acid	783.7	117.5	220.4 [c]	-	-	38.6	-	-

	HCN_1	Acetonitrile	C_2H_3N	41	Cyanide / nitrile	779.2	81.2	328.8 [c]	86.0	49.5	53.1	32.1	30.9
	HCN_1O_2	Nitrobenzene	$C_6H_5NO_2$	123	Nitro	800.3	210.3	-	88.8	-	-	20.3	-
Nonpolar compound	HC	Isoprene	C_5H_8	68	Diene	826.4	33.7	82.4 [c]	35.7	25.8	29.2	17.7	16.1
		Benzene	C_6H_6	78	Aromatic	750.4	79.7	197.2 [c]	61.6	25.0	23.3	16.6	15.6
		Toluene	C_7H_8	92	Aromatic	784.0	110.1	231.6 [c]	75.6	35.0	26.0	19.1	21.9
		o-Xylene	C_8H_{10}	106	Aromatic	796.0	143.9	269.2 [c]	87.9	10.2	27.1	20.2	6.4
		1,2,4-Trimethylbenzene (1,2,4-TMB)	C_9H_{12}	120	Aromatic	-	168.9	274.4 [c]	93.8	-	25.9	20.2	-

a Obtained using Eq. (7-a) involving the detected ion intensities of VOC·H+ and H3O+. b Obtained using Eq. (8). c Reported in reference [7].

Table 2.2

Measured sensitivity in PTR-MS vs. kinetic reaction rate constant

(a) Volatile organic compound (VOC)					(c) Product ion distribution								(d) Measured polarizability [30] :	(e) Measured permanent dipole moment [30] :	(f) Kinetic reaction rate constant : $k_{kinetic}$ [x 10^{-9} cm^3 $molecule^{-1}$ s^{-1}] [d]	
	HCP_m		Formula	Molecular mass M_R [Da]	H_3O^+-ToF-CIMS		Modified H_3O^+-ToF-CIMS		PTR-QMS [27]						E/N = 120 Td, T_{DT} = 323 K [e]	E/N = 106 Td, T_{DT} = 323 K [e]
					Ion formula (m/z)	Fraction [%]	Ion formula (m/z)	Fraction [%]	Ion formula (m/z)	Fraction [%]			$\alpha_{meas.}$ [x 10^{-24} cm^3]	$\mu_{D\ meas.}$ [D]	((Modified) H_3O^+-ToF-CIMS)	(PTR-QMS)
Polar compound	HCO_1	Methanol	CH_4O	32	CH_5O^+ (33)	97	CH_5O^+ (33)	90	CH_5O^+ (33)	100			3.28	1.70	2.30	2.35
					CH_3^+ (15)	2	H_3O^+ (19)	8								
					Others	1	CH_3^+ (15)	2								
		Acetaldehyde	C_2H_4O	44	C	99	C_2	99	C	100			4.60	2.75	3.09	3.1

					$_2H_5O^+$ (45)			H_5O^+ (45)			$_2H_5O^+$ (45)											6
					Others	1		Others	1													
		Ethanol	C_2H_6O	46	$C_2H_7O^+$ (47)	93		-			$C_2H_7O^+$ (47)	50			5.26	1.69		2.31	2.40			
					$C_2H_5^+$ (29)	7					$C_2H_5^+$ (29)	50										
		Acrolein	C_3H_4O	56	-			$C_3H_5O^+$ (57)	96		-				6.38	2.83		3.14	3.29			
								Others	4													
		Acetone	C_3H_6O	58	$C_3H_7O^+$ (59)	96		$C_3H_7O^+$ (59)	96		$C_3H_7O^+$ (59)	90			6.37	2.88		3.23	3.31			
					CH_3O^+ (31)	3		CH_3O^+ (31)	3		$C_3H_7^+$ (43)	10										
					Others	1		Others	1													
		Methyl ethyl ketone (MEK)	C_4H_8O	72	$C_4H_9O^+$ (73)	94		$C_4H_9O^+$ (73)	94		$C_4H_9O^+$ (73)	100			8.13	2.78		3.21	3.30			
					$C_2H_5O_2^+$ (61)	2		$C_2H_5O_2^+$ (61)	2													
					$C_2H_5O^+$ (45)	1		$C_2H_5O^+$ (45)	1													
					Others	3		Others	3													

					thers				thers													
	Anisole	C_7H_8O	108		-				$C_7H_9O^+$ (109)	96			-				13.10	1.38		2.23	2.38
									Others	4												
HCO_2	Formic acid	CH_2O_2	46		$CH_3O_2^+$ (47)	97			-				-				3.40	1.43		1.92	1.98
					Others	3																
	Acetic acid	$C_2H_4O_2$	60		$C_2H_5O_2^+$ (61)	76			-				-				5.10	1.70		2.20	2.29
					$C_2H_3O^+$ (43)	24																
	HCN_1	Acetonitrile	C_2H_3N	41		$C_2H_4N^+$ (42)	99			$C_2H_4N^+$ (42)	98			$C_2H_4N^+$ (42)	100			4.44	3.93		3.98	4.11
						Others	1			Others	2											
	HCN_1O_2	Nitrobenzene	$C_6H_5NO_2$	123		-				$C_6H_6NO_2$ (124)	93			-				13.81	4.22		4.25	4.47
										C_6H_6 (78)	1											
										Others	6											
Nonpolar	HC	Isoprene	C_5H_8	68		$C_5H_9^+$	35			$C_5H_9^+$	58			$C_5H_9^+$	100			9.99	0.25		1.92	1.92

compound					(69)			(69)			(69)									
					$C_5H_7^+$ (67)	2		Others	32											
					$C_3H_5^+$ (41)	56														
					Others	7														
		Benzene	C_6H_6	78	$C_6H_7^+$ (79)	99		$C_6H_7^+$ (79)	99		$C_6H_7^+$ (79)	100			10.35	0.00		1.93	1.93
					Others	1		Others	1											
		Toluene	C_7H_8	92	$C_7H_9^+$ (93)	96		$C_7H_9^+$ (93)	97		$C_7H_9^+$ (93)	100			12.12	0.38		2.05	2.05
					$C_7H_7^+$ (91)	4		$C_7H_7^+$ (91)	3											
		o-Xylene	C_8H_{10}	106	$C_8H_{11}^+$ (107)	100		$C_8H_{11}^+$ (107)	100		$C_8H_{11}^+$ (107)	100			14.50	0.64		2.22	2.22
		1,2,4-Trimethylbenzene (1,2,4-TMB)	C_9H_{12}	120	$C_9H_{13}^+$ (121)	100		$C_9H_{13}^+$ (121)	100		-				17.17	0.33		2.39	2.39

d Calculated by substituting (d) ameas. and (f) mD meas. in Eqs. (11) and (13). e TDT represents the drift tube temperature.

Table 3

Polarizability α										
Compound R					**(d) Linear function to obtain $\alpha(M_R, HCP_m)$ [x 10^{-24} cm^3]**		**(e) $\alpha(M_R)$ [x 10^{-24} cm^3] [d]**		**Relative error [%] [e]**	
(a) HCP_m	**(b) Total number (M_R range)**	**(c) Chemical class (number)**			**$\alpha_{literature}$ [x 10^{-24} cm^3] = $b\,M_R$ [Da] + c (Correlation coefficient : r)**	**Exception**			**(f) $\alpha(M_R, HCP_m)$**	**(g) $\alpha(M_R)$ [f]**
HC	**118 (M_R = 16-300)**	**Alkane**	**(18)**		**α = (0.142 ± 0.002) M_R - (0.3 ± 0.3) (r = 0.9838)**	**Azulene, phenanthrene, pyrene, fluoranthene, naphthacene**	**α = (0.13 ± 0.01) M_R - (1.3 ± 1.0)**		**4.6**	**16.7**
		Alkene	**(17)**							
		Alkyne	**(9)**							
		Diene	**(10)**							
		Cyclo-alkane, alkene and								
		iene	**(17)**							
		Bicyclo-alkane and alkene	**(6)**							

		Aromatic	**(20)**									
		Polyaromatic	**(19)**									
		Others	**(2)**									
HCO_1	**55 (M_R = 30-198)**	**Ketone / aldehyde**	**(24)**		**α = (0.133 ± 0.002) M_R - (1.2 ± 0.2) (r = 0.9946)**	**-**				**3.9**	**5.1**
		Alcohol / phenol	**(15)**									
		Ether	**(11)**									
		Furan	**(2)**									
		Epoxide	**(2)**									
		Others	**(1)**									
HCO_2	**35**	**Ester**	**(11**		**α = (0.142 ±**	**-**				**5.5**	**15.0**

	(M_R = 46-208)		)		0.005) M_R - (3.4 ± 0.5) (r = 0.9786)						
		Carboxylic acid	(5)								
		Quinone	(3)								
		Others	(16)								
$HCO_{3 \text{ or } 4}$	7 (M_R = 90-174)	Carbonate	(2)		α = (0.12 ± 0.03) M_R - (2.11 ± 4.35) (r = 0.8398)	Paraldehyde				9.4	26.2
		Others	(5)		α = (0.110 ± 0.006) M_R - (2.0 ± 0.8) [a] (r = 0.9932)					2.7 [a]	
HCN_1	30 (M_R = 31-143)	Cyanide / nitrile	(10)		α = (0.129 ± 0.005) M_R + (0.2 ± 0.5) (r = 0.9773)	Butylamine				7.0	13.7
		Primary amine	(8)		α = (0.131 ± 0.004) M_R - (0.1 ± 0.3) [b]					6.4 [b]	
		Secondary amine	(3)								

		Tertiary amine	(4)		(r = 0.9897)						
		Pyridine	(1)								
		Quinoline	(4)								
HCN_2	20 (M_R = 52-180)	Others	(20)		α = (0.13 ± 0.01) M_R - (1.2 ± 1.1) (r = 0.9536)	Cyanogen, fumaronitrile, *p*-dicyanobenzene			10.8	10.0
HCN_pO_q (p = 1, 2, 4; q = 1-4, 8)	18 (M_R = 45-215)	Amide	(5)		α = (0.104 ± 0.009) M_R + (0.2 ± 1.1) (r = 0.9468) α = (0.119 ± 0.006) M_R - (1.0 ± 0.6) [c] (r = 0.9833)	Tetranitromethane			10.2 7.3 [c]	14.4
		Nitro	(6)								
		Others	(7)								
HCS_1	5 (M_R = 62-90)	Sulfide	(3)		α = (0.14 ± 0.02) M_R - (1.4 ± 1.3) (r = 0.9770)	-			3.6	5.0
		Thiol	(1)								

			)								
		Thiophene	(1)								
Overall HCP_m	-	-			-	-		-		5.6 [g]	13.3 [g]

a Except for paraldehyde. b Except for butylamine. c Except for tetranitromethane. d Slope and intercept were obtained by averaging coefficients c and d in the equations for individual HCPm categories shown in (d).

e $\text{Relative error} = \{|a(M_R, HCP_m) \text{ or } a(M_R) - a_{meas.}|) / a_{meas.} \times 100 [\%]$

f Exceptions described in (d) were included.

g Error of a(MR, HCPm) or a(MR) for overall HCPm, which is obtained by averaging the average relative errors (REave.) of individual HCPm categories: $\text{Error} = \overline{\Sigma RE_{ave.}}$

Table 4.1

Permanent dipole moment μ_D

Compound R					Estimated dipole moment *K* [D]			Relative error [%] [d]		
(a) HCP_m	(b) Functional group (Total number, M_R range)	(c) Chemical property of residual hydrocarbon part (number)			(d) From functional group; μ_D (FG) [a] (exception)	(e) From elemental composition; μ_D (HCP_m) [b]	(f) From molecular mass; μ_D (M_R) [c]	(g) μ_D (FG) [e]	(h) μ_D (HCP_m) [f]	(i) μ_D (M_R) [f]
HCO_1	Ketone / aldehyde (37, M_R = 30-152)	Chain/saturated aliphatic	(18)		2.8 ± 0.2 (Formaldehyde, *trans*-2-butenal 3-methyl-2-cyclopenten-1-one, 2,4,6-cycloheptatrien-1-one)	1.6 ± 0.7	2.1 ± 0.9	5.8	42.4	27.9
		Chain/unsaturated aliphatic	(6)							
		Cyclic/saturated aliphatic	(7)							
		Cyclic/unsaturated aliphatic	(3)							
		Aromatic + chain/saturated aliphatic	(2)							
		Non-benzenoid aromatic	(1)							

	Alcohol / phenol (35, M_R = 32-130)		**Alcohol : Chain/saturated aliphatic**	**(18)**		**1.6 ± 0.2**				**9.5**	**9.5**	**29.5**
			Chain/unsaturated aliphatic	**(5)**								
			Cyclic/saturated aliphatic	**(2)**								
			Aromatic + chain/saturated aliphatic	**(1)**								
			Phenol : Chain/saturated aliphatic	**(9)**								
	Ether (19, M_R = 46-170)		**Chain/saturated aliphatic**	**(11)**		**1.2 ± 0.2**				**10.4**	**42.3**	**78.2**
			Chain/unsaturated aliphatic	**(5)**								
			Aromatic + chain/saturated aliphatic	**(2)**								
			Aromatic	**(1)**								
	Epoxide		**Chain/saturated aliphatic**	**(3**		**1.93 ± 0.06**				**2.7**	**14.5**	**7.1**

	(3, M_R = 44-72)			)							
	Furan (4, M_R = 68-94)		Chain/saturated aliphatic	(3)		0.73 ± 0.08			14.5	125.6	182.6
			Chain/unsaturated aliphatic	(1)							
	Others (8, M_R = 42-86)	-				-			-	14.2	36.5
	Overall HCO_1	-				-	-		8.6[g]	41.4[g]	60.3[g]
HCO_2	Ester (30, M_R = 60-340)		Chain/saturated aliphatic	(20)		1.8 ± 0.1 (Benzyl acetate)	1.9 ± 0.5		5.0	8.6	14.6
			Chain/unsaturated aliphatic	(5)							
			Aromatic + chain/saturated aliphatic	(4)							
			Aromatic + chain/unsaturated aliphatic	(1)							

Carboxylic acid (13, M_R = 46-282)		**Chain/saturated aliphatic**	**(10)**		**1.4 ± 0.4**			**29.3**	**56.7**	**66.1**
		Chain/unsaturated aliphatic	**(3)**							
Others (38, M_R = 46-138)		**-**			**-**			**-**	**44.0**	**43.5**
	Overall HCO_2		**-**			**-**	**-**		**17.2** [g]	**36.4** [g]	**41.4** [g]
HCO_3	**Others (15, M_R = 88-152)**		**-**			**-**	**2.4 ± 1.1**		**-**	**32.4**	**27.3**
HCO_4	**Others (8, M_R = 144-390)**		**-**			**-**	**2.5 ± 0.3**		**-**	**9.0**	**18.7**

a $\overline{m_D(\mathrm{FG})_{\mathrm{meas.}}}$ ± standard deviation : Exceptions described in parentheses were excluded. In the case of regio-isomers and/or stereo-isomers, average mD meas. for those were used.

b $m_D(\mathrm{HCP}_m) = \sum m_D(\mathrm{FG}) + \overline{m_{D,\mathrm{meas.}}(\mathrm{Others})}$ ± standard deviation : In the case of regio-isomers and/or stereo-isomers, average mD meas. for those were used.

$$\propto_D(M_R) \pm \sqrt{\propto_D(HCP_m)^2 + \propto_D(HC)^2}$$

c ± standard deviation : mD(HC) = 0

d Relative error = $\left[\left(\propto_D(FG, HCP_m, \text{or } M_R) - \propto_{D\,meas.}\right) / \propto_{D\,meas.}\right] \times 100\ [\%]$

e Exceptions described in parentheses in (d) were excluded.

f Exceptions described in parentheses in (d) were included.

$$\text{Error} = \sqrt{\sum RE_{ave.}}$$

g Error of mD(FG), mD(HCPm) or mD(MR) in each HCPm category, which is obtained by averaging the average relative error (REave.) of appropriate functional group categories:

Table 4.2

Permanent dipole moment μ_D

Compound R			Estimated dipole moment *K* [D]			Relative error [%] [d]		
(a) HCP_m	(b) Functional group (Total number, M_R range)	(c) Chemical property of residual hydrocarbon part (number)	(d) From functional group; μ_D (FG) [a] (exception)	(e) From elemental composition; μ_D (HCP_m) [b]	(f) From molecular mass; μ_D (M_R) [c]	(g) μ_D (FG) [e]	(h) μ_D (HCP_m) [f]	(i) μ_D (M_R) [f]
HCN_1	Cyanide / nitrile (16, M_R = 27-117)	Chain/saturated aliphatic (9)	4.0 ± 0.3 (Hydrogen cyanide)		2.1 ± 0.9	5.6	46.2	46.3
		Chain/unsaturated aliphatic (4)						
		Cyclic/saturated aliphatic (1)						
		Aromatic + chain/saturated aliphatic (1)						
		Aromatic (1)						
	Isocyanide (4, M_R = 27-103)	Chain/saturated aliphatic (2)	4.03 ± 0.02 (Hydrogen isocyanide)			0.3	44.5	44.7
		Cyclic/saturated aliphatic (						

				1)									
			Aromatic	(1)									
	Primary amine (18, M_R = 31-121)		Chain/saturated aliphatic	(9)		1.3 ± 0.1	2.1 ± 1.3			9.1	61.7	61.2
			Chain/unsaturated aliphatic	(1)									
			Cyclic/saturated aliphatic	(2)									
			Aromatic + chain/saturated aliphatic	(5)									
			Aromatic	(1)									
	Secondary amine (5, M_R = 45-129)		Chain/saturated aliphatic	(5)		1.02 ± 0.08				5.6	104.6	103.9
	Tertiary amine (4, M_R = 59-121)		Chain/saturated aliphatic	(3)		0.68 ± 0.07 (*N*,*N*-				9.2	160.3	159.5

			Aromatic + chain/saturated aliphatic	(1)		Dimethylaniline)							
	Pyridine (7, M_R = 79-121)		Chain/saturated aliphatic	(7)		2.1 ± 0.1			13.0	13.0	13.0
	Others (11, M_R = 43-129)	-				-			-	67.4	67.0
	Overall HCN_1	-				-	-		7.1 [g]	71.1 [g]	70.8 [g]
HCN_2	**Others** (13, M_R = 42-104)	-				-	3.0 ± 0.9		-	39.4	32.0
HCN_1O_q (q = 1, 2)	**Amide** (7, M_R = 45-87)		Chain/saturated aliphatic	(7)		3.8 ± 0.2	3.5 ± 0.4		3.8	9.1	45.6
	Nitro		Chain/saturated aliphatic	(4		3.7 ± 0.4			6.9	7.7	43.1

	(5, M_R = 61-123)			)							
			Aromatic	(1)							
	Others (22, M_R = 43-113)	-				-			-	60.2	36.7
	Overall HCN_1O_q	-				-	-		5.4 [g]	25.7 [g]	41.8 [g]
HCS_1	Sulfide (7, M_R = 62-146)		Chain/saturated aliphatic	(7)		1.58 ± 0.02	1.589 ± 0.008		1.7	1.7	30.2
	Thiol (10, M_R = 48-110)		Chain/saturated aliphatic	(9)		1.58 ± 0.05 (Benzenethiol)			2.9	5.5	33.7
			Aromatic	(1)							
	Others (10, M_R = 46-98)	-				-			-	49.7	71.2

	Overall HCS_1	-			-	-			**2.3** [g]	**19.0** [g]	**45.0** [g]

a $m_D(FG) = \overline{m_{D,meas.}}$ **± standard deviation : Exceptions described in parentheses were excluded. In the case of regio-isomers and/or stereo-isomers, average mD meas. for those were used.**

b $m_D(HCP_m) = \overline{\sum m_D(FG) + m_{D,meas.}(Others)}$ **± standard deviation : In the case of regio-isomers and/or stereo-isomers, average mD meas. for those were used.**

c $\propto_D (M_R) = \overline{\sum \propto_D (HCP_m) + \propto_D (HC)}$ **± standard deviation : mD(HC) = 0**

d Relative error = $\overline{(|\propto_{DE}(FG, HCP_m, or M_R) - \propto_{D meas.}|) / \propto_{D meas.}} \times 100 [\%]$

e Exceptions described in parentheses in (d) were excluded

.f Exceptions described in parentheses in (d) were included.

g Error of mD(FG), mD(HCPm) or mD(MR) in each HCPm category, which is obtained by averaging the average relative error (REave.) of appropriate functional group categories:

$$\text{Error} = \overline{\sum RE_{ave.}}$$

Table 5

Capture rate constant k_{cap}

Compound R whose $k_{meas.}$ is used									Relative error of $k_{cap}[\alpha, \mu_D]$ [%] [a] (number)									
	(a) HCP_m	(b) Functional group	(Total number, M_R range)		(c) Chemical property of residual hydrocarbon part	(number)		[α, μ_D] =	(d) [$\alpha_{meas.}$, $\mu_{D\ meas.}$] [b]		(e) [$\alpha(M_R$, HCP_m), μ_D(FG)] [c]		(f) [$\alpha(M_R$, HCP_m), μ_D(HCP_m)]		(g) [$\alpha(M_R)$, $\mu_D(M_R)$]	
			Thermal	Kinetic		Thermal	Kinetic		Thermal	Kinetic	Thermal	Kinetic	Thermal	Kinetic	Thermal	Kinetic
Polar compound	HCO_1	Ketone / aldehyde	(18, M_R = 30-154)	(4, M_R = 44-72)	Chain/saturated aliphatic	(13)	(3)		4.8 (7)	5.4 (3)	9.1 (18)	5.3 (4)	22.8 (18)	30.1 (4)	14.6 (18)	19.8 (4)
					Chain/unsaturated aliphatic	(2)	(1)									
					Cyclic/saturated aliphatic	(1)	(0)									
					Aromatic + chain/saturated aliphatic	(1)	(0)									
					Aromatic	(1)	(0)									
		Alcohol / phenol	(17, M_R = 32-156)	(2, M_R = 32-86)	Alcohol : Chain/saturated aliphatic	(15)	(1)		3.9 (8)	2.1 (2)	6.1 (17)	1.4 (2)	6.7 (17)	0.7 (2)	18.9 (17)	13.4 (2)
					Chain/unsaturated	(0)	(1)									

					aliphatic															
					Cyclic/saturated aliphatic	(1)	(0)													
					Phenol : Chain/saturated aliphatic	(1)	(0)													
	Ether	(8, M_R = 74-108)	-		Chain/saturated aliphatic	(6)	-			8.9 (3)	-		7.2 (8)	-		19.7 (8)	-		31.9 (8)	-
					Chain/unsaturated aliphatic	(1)														
					Aromatic + chain/saturated aliphatic	(1)														
	Others; tetrahydrofuran	(1, M_R = 72)	-		Chain/saturated aliphatic	(1)	-			-	-		-	-		2.9 (1)	-		15.8 (1)	-
	Overall HCO_1			-						5.9 [d]	3.7 [d]		7.5 [d]	3.3 [d]		13.0 [d]	15.4 [d]		20.3 [d]	16.6 [d]
HCO_2	Ester	(8, M_R = 60-136)	-		Chain/saturated aliphatic	(7)	-			2.4 (5)	-		6.5 (8)	-		8.9 (8)	-		15.7 (8)	-
					Aromatic + chain/saturated aliphatic	(1)														

	Carboxylic acid	(8, M_R = 46-102)	-		Chain/saturated aliphatic	(7)	-			3.8 (4)	-		5.5 (8)	-		13.4 (8)	-		21.5 (8)	-
					Chain/unsaturated aliphatic	(1)														
	Others; ketone/ketone, alcohol/alcohol	(2, M_R = 86-90)	-		Chain/unsaturated aliphatic	(2)	-			-	-		-	-		50.1 (2)	-		59.5 (2)	-
	Overall HCO_2			-						3.1 [d]	-		6.0 [d]	-		24.1 [d]	-		32.3 [d]	-
HCN$_1$	Cyanide / nitrile	(2, M_R = 41-103)	(1, M_R = 41)		Chain/saturated aliphatic	(1)	(1)			5.2 (2)	1.3 (1)		4.3 (2)	1.6 (1)		34.8 (2)	32.8 (1)		36.8 (2)	36.3 (1)
					Aromatic	(1)	(0)													
	Primary amine	(5, M_R = 59-93)	-		Chain/saturated aliphatic	(4)	-			4.3 (4)	-		3.7 (5)	-		29.5 (5)	-		25.8 (5)	-
					Aromatic	(1)														

		Secondary amine	(3, M_R = 45-73)	-		Chain/saturated aliphatic	(3)	-		9.3 (2)	-		6.8 (3)	-		47.8 (3)	-		43.3 (3)	-
		Tertiary amine	(2, M_R = 59-101)	-		Chain/saturated aliphatic	(2)	-		3.8 (2)	-		4.5 (2)	-		52.1 (2)	-		47.9 (2)	-
		Pyridine	(1, M_R = 79)	-		Chain/saturated aliphatic	(1)	-		4.4 (1)	-		4.1 (1)	-		2.2 (1)	-		0.6 (1)	-
		Others; pyrrole	(1, M_R = 67)	(1, M_R = 67)		Chain/saturated aliphatic	(1)	(1)		-	-		-	-		10.5 (1)	0.2 (1)		7.3 (1)	2.5 (1)
		Overall HCN_1			-					5.4 [d]	1.3 [d]		4.7 [d]	1.6 [d]		29.5 [d]	16.5 [d]		27.0 [d]	19.4 [d]
	HCS [1]	Sulfide	(4, M_R = 62-90)	-		Chain/saturated aliphatic	(3)	-		4.0 (1)	-		3.9 (4)	-		4.0 (4)	-		17.9 (4)	-
						Chain/unsaturated aliphatic	(1)													
		Thiol	(1, M_R = 62)	-		Chain/saturated aliphatic	(1)	-		7.4 (1)	-		5.8 (1)	-		6.0 (1)	-		23.0 (1)	-

		Overall HCS_1			-					**5.7 [d]**	**-**		**4.8 [d]**	**-**		**5.0 [d]**	**-**		**20.5 [d]**	**-**
		Overall polar compounds			-					**5.2 [d]**	**2.9 [d]**		**5.6 [d]**	**2.7 [d]**		**20.8 [d]**	**15.9 [d]**		**25.4 [d]**	**18.0 [d]**
Nonpolar compound	**HC**	**-**	**(29, M_R = 40-142)**		**Alkane**	**(2)**			**6.1 [e] (15)**			**6.5 [e] (25)**			**-**			**63.7 [e] (25)**	
					Alkene	**(10)**														
					Alkyene	**(1)**														
					Diene	**(1)**														
					Cycloalkane	**(2)**														
					Bicycloalkene	**(4)**														
					Aromatic	**(9)**														

a **Average relative error = $\overline{(|k_{cap} - k_{meas.}|) / k_{meas.}}$ X 100 [%]**

b kcap[ameas., mD meas.] for HC corresponds to kcap[ameas.].

c kcap[a(MR, HCPm), mD(FG)] for HC corresponds to kcap[a(MR, HCPm)].

d Error of kcap[a, mD] in each HCPm category or overall polar compounds, which is obtained by averaging the average relative errors (REave.) of appropriate functional group categories:

Error = $\overline{RE_{ave.}}$

e (Cyclo)alkanes were excluded.

Table 6

Calculated vs. measured sensitivity in PTR-MS

(a) Volatile organic compound (VOC)								(b) Measured sensitivity [ncps ppbv^{-1}] [a]		(c) Sensitivity calculated using capture rate constant $k_{cap}[\alpha, \mu_D]$ [ncps ppbv^{-1}] (corresponding relative error [%] with respect to measured sensitivity)				
	HCP_m		Formula	Molecular mass M_R [Da]	Functional group / chemical group	Proton affinity [kJ mol^{-1}] [11]	Vapor pressure [°C at 100 kPa] [30]	H_3O^+-ToF-CIMS	Modified H_3O^+-ToF-CIMS	[α, μ_D] =	(I) [$\alpha_{meas.}$, $\mu_{D\ meas.}$] [b]	(II) [$\alpha(M_R$, HCP_m), μ_D(FG)] [c]	(III) [$\alpha(M_R$, HCP_m), μ_D(HCP_m)]	(IV) [$\alpha(M_R$), $\mu_D(M_R$)]
Polar compound	HCO_1	Pentanone	$C_5H_{10}O$	86	Ketone	834.8	101.8	46.1	-		44.9 (2.6) [e]	45.7 (0.8)	30.2 (30.0)	36.4 (21.0)
		Hexanone	$C_6H_{12}O$	100	Ketone	-	125.2	40.7	-		44.1 (8.3) [e]	46.2 (13.4)	33.3 (18.1)	36.8 (9.5)
		Phenol	C_6H_6O	94	Phenol	817.3	181.4	-	14.4		19.4 (35.1)	21.3 (48.1)	21.4 (48.9)	23.8 (65.9)
		Cresol	C_7H_8O	108	Phenol	818.3	197.9	-	14.7		21.4 (45.5)	22.0 (49.9)	22.1 (50.6)	24.2 (64.8)
		Furan	C_4H_4O	68	Furan	803.4	31.0	23.5	-		24.4 (3.6) [e]	24.6 (4.6)	31.2 (32.9)	36.2 (54.0)
		2-Methylfuran	C_5H_6O	82	Furan	865.9	64.5	-	17.0		17.1 (1.0) [e]	17.3 (1.9)	20.8 (22.7)	23.7 (39.5)
	HCO_2	Furfural	$C_5H_4O_2$	96	Others	-	161.4	-	30.3		33.9 (11.8)	-	22.5 (25.7)	23.8 (21.7)
	HCN_1	Pyridine	C_5H_5N	79	Pyridine	930.0	114.9	31.7	-		38.4 (21.2)	37.9 (19.8)	37.1 (17.1)	36.3 (14.7)
	HCN_1O_1	Methyl isocyanate	C_2H_3NO	57	Others	764.4	38.8	42.0	-		43.1 (2.6) [e]	-	49.3 (17.3)	36.0 (14.4)

	Overall polar compounds												**$RE_{ave.}$ = 14.6 %[d]**	**$RE_{ave.}$ = 19.8 %[d]**	**$RE_{ave.}$ = 29.2 %[d]**	**$RE_{ave.}$ = 34.0 %[d]**
Nonpolar compound	**HC**	**Ethylbenzene**	**C_8H_{10}**	**106**	**Aromatic**	**788.0**	**135.7**		**-**	**14.9**			**19.7 (32.7)**	**20.1 (35.5)**	**-**	**24.2 (62.4)**
		α-Methylstyrene	**C_9H_{10}**	**118**	**Aromatic**	**864.2**	**164.9**		**-**	**20.6**			**20.8 (1.0)**	**21.1 (2.4)**	**-**	**24.6 (19.2)**
		***p*-Cymene**	**$C_{10}H_{14}$**	**134**	**Aromatic**	**-**	**176.6**		**-**	**18.9**			**-**	**22.3 (18.0)**	**-**	**25.2 (33.4)**
		α-Pinene	**$C_{10}H_{16}$**	**136**	**Bicycloalkene**	**-**	**155.1**		**31.9**	**-**			**-**	**34.5 (8.2)**	**-**	**38.9 (21.9)**
	Overall nonpolar compounds												**$RE_{ave.}$ = 16.9 %[d]**	**$RE_{ave.}$ = 16.0 %[d]**	**-**	**$RE_{ave.}$ = 34.3 %[d]**

a Corrected for fragmentation and ion transmission efficiencies via Eq. (8). b kcap[ameas., mD meas.] for HC corresponds to kcap[ameas.]. c kcap[a(MR, HCPm), mD(FG)] for HC corresponds to kcap[a(MR, HCPm)]. d REave. represents the average relative error in each rate constant category.

e Using a(MR, HCPm) because of no data of ameas.